HOKKAIDO UNIVERSITY

| | |
|---|---|
| Title | Development of Guidance System Using Local Sensors for Agricultural Vehicles |
| Author(s) | 崔, 鍾民 |
| Citation | 北海道大学. 博士(農学) 甲第11393号 |
| Issue Date | 2014-03-25 |
| DOI | 10.14943/doctoral.k11393 |
| Doc URL | http://hdl.handle.net/2115/56098 |
| Type | theses (doctoral) |
| File Information | Choi_Jongmin.pdf |

Instructions for use

Hokkaido University Collection of Scholarly and Academic Papers : HUSCAP

# Development of Guidance System Using Local Sensors for Agricultural Vehicles

# ローカルセンサを用いた農用車両用ガイダンスシステムの開発

2014

北海道大学　　大学院農学院

環境資源学専攻　　博士後期課程

崔 鍾民

Choi Jongmin

# Development of Guidance System Using Local Sensors for Agricultural Vehicles


BY

Choi Jongmin

**DISSERTATION**

*Submitted to Department of Environmental Resources in the Graduate School of Agriculture*

*Hokkaido University, Sapporo, Japan, 060-8589 in partial fulfillment of the requirements for the degree of*

*Doctor of Philosophy*

*2014*

# TABLE OF CONTENTS

# ACKNOWLEDGEMENTS

I would like to express my deepest sense of gratitude to my supervisor Professor Noboru Noguchi for his patient guidance, encouragement and excellent advice throughout this study.

I also would like to express thank to Professor Han Chungsu and professor Kang Taehwan for moral support.

I also would like to thank to Dr. Kazunobu Ishii who has given me many creative ideas and methods. And give thanks to Dr. Hiroshi Okamoto and Dr. Liangliang Yang who have helped me a lot on the preparing of this thesis. And give thanks to Dr. Yoichi Shibata for valuable discussions during research.

I am thankful to my colleagues in the laboratory of vehicle robotics who are Dr. Xiang Yin, Dr. Ze Zhang, Ryosuke Takai. Thank you giving me great encouragement, cooperation and helps for the field tests.

# DEDICATION

To my family, my beloved wife whose love contributes strength for me to finish my PhD research.

# LIST OF FIGURES

# LIST OF TABLES

# NOTATION

| | | |
|---|---|---|
| $a, b, c$ | The straight line coefficients | |
| $A_1, A_2$ | The Corresponding gains | |
| $E$ | Rotation matrix | |
| $E_{x180}$ | Rotation matrix around X axis for 180° | |
| $E_{z\psi}$ | Rotation matrix around Z axis for ψ° | |
| $H$ | Height of the laser scanner origin $O_L$ | [m] |
| $h$ | Height of crop plants | [m] |
| $K_1, K_2, K_3$ | Distortion constants | |
| $O_L, X_L, Y_L, Z_L$ | Coordinates under laser scanner scan plane coordinate system | |
| $P_1$ | Crop plant location detected at a tilt angle of 48 degrees | |
| $P_2$ | Crop plant location detected at a tilt angle of 69egrees | |
| $P_x, P_y$ | Defining principal point | |
| $x, y$ | Destination coordinates | |
| $X_{cGPS1}$ | Initial coordinates of the camera origin | |
| $X_d, Y_d$ | Coordinates in distorted image | |
| $X_r, Y_r$ | Coordinates in rectified image | |
| $X_{tGPS1}, Y_{tGPS1}, Z_{tGPS1}$ | Initial coordinates of the tractor origin | |
| $X_{wc}, Y_{wc}, X_{wc}$ | Coordinates under the camera coordinate system | |

*Notation*

| | | |
|---|---|---|
| $X_{wGPS1}$, $Y_{wGPS1}$, $Z_{wGPS1}$ | Coordinate of GPS1 in the world reference frame | |
| $X_{wt}$, $Y_{wt}$, $X_{wt}$ | Coordinates under the tractor coordinate system | |
| $X_w$, $Y_w$, $X_w$ | UTM coordinate system | |
| $X_V$, $Y_V$, $Z_V$, $O_V$ | The combine harvester Cartesian coordinate system | |
| $B$ | The angle between the scanning plane $X_L O_L Y_L$ | [ deg ] |
| $\Delta$ | Deflection angle | [ deg ] |
| $\delta_a$ | Actual deflection angle | [ deg ] |
| $E$ | Lateral offset | [ m ] |
| $\varepsilon$ | Lateral error | [ m ] |
| $\varepsilon_a$ | Actual lateral offset | [ m ] |
| $\theta_t$ | Roll angle of tractor | [ deg ] |
| $\theta$ | The angle of the beam direction away from the origin axis $O_L X_L$ | [ deg ] |
| $\theta_{ini}$ | Roll angles of the IMU | [ deg ] |
| $\rho_t$ | Pitch angle of tractor | [ deg ] |
| $\rho$ | Distance between the laser scanner reference origin and the object | [ m ] |
| $\rho_{ini}$ | Pitch angles of the IMU | [ deg ] |
| $\varphi$ | Steering angle of combine harvester | [ deg ] |
| $\psi$ | Yaw angle of tractor | [ deg ] |

# ACRONYMS AND ABBREVIATIONS

| | |
|---|---|
| 3D | Three Dimensional |
| ACPA | Asian Conference on Precision Agriculture |
| AR | Augmented Reality |
| CAN | Controller Area Network |
| CGI | Computer-generated image |
| CCD | Charge-coupled Device |
| DC | Direct Current |
| DGPS | Differential Global Positioning System |
| ECU | Electronic Control Unit |
| FDS | Full-time Drive System |
| FOG | Fiber Optic Gyroscope |
| FOV | Field of View |
| GIS | Geographical Information System |
| GPS | Global Positioning System |
| HST | Hydraulic Static Transmissions |
| IMU | Inertial Measurement Unit |
| ISPA | International Society of Precision Agriculture |
| LS | Laser Scanner |

| | |
|---|---|
| PA | Precision Agriculture |
| PC | Personal Computer |
| PD | Proportional-Derivative |
| PID | Proportional-Integral-Derivative |
| RMS | Root Mean Square |
| PTO | Power take off |
| PTU | Pan-Tilt Unit |
| RS232C | Recommended Standard 232C |
| RTK-GPS | Real-time Kinematic–Global Positioning System |
| US | United States |
| UTM | Universal Transverse Mercator |
| VRS-RTK-GPS | Virtual Reference Station–Real-time Kinematic–Global Positioning System |

# CHAPTER 1

# INTRODUCTION

## 1.1 Research background

Nowadays, the world's growing population brings about the problem of food shortage that comes to be of great urgency all over the world. And a consequent challenge rises in modern agriculture. It needs to be realized that more outputs could be extracted from the environment by using less inputs. Simultaneously, a comprehensive consideration of environment protection should be taken so that a sustainable agricultural production could be witnessed in following centuries. Another problem in agricultural production is the decreasing workforce, especially in developed countries like Japan.

In modern agriculture, a guidance system of agricultural vehicles has received the attention of researchers. From a review of the literature, several motivations are apparent from the effort that has been expended towards the development of a guidance system, be it autonomous or partially autonomous. The rapid advancement in electronics, computers, and computing technologies has inspired renewed interests in the development of guidance systems. Various guidance technologies, including mechanical guidance, optical guidance, radio navigation, and ultrasonic guidance, have been investigated (Reid *et al*., 2000; Tillett, 1991). In general, any guidance technology will need to provide positioning information of the vehicle, referenced either in a global coordinate system or in a local coordinate system.

### 1.1.1 Agricultural autonomous vehicles

In this thesis, a guidance system refers to a system that show target path and current position of a vehicle via a User Interface. An auto guidance (or auto steering) system is an auto steering controlling system for a vehicle using a guidance system. And a robot vehicle is an autonomous vehicle of which the steering, engine rotation, vehicle speed, PTO, Hitch etc. of a vehicle can be controlled automatically.

With intensive application of techniques in global positioning, machine vision, image processing, sensor integration and computing-based algorithms, the vehicle automation has evolved from a concept to be an existence worldwide. Figure 1.1 shows a wheel-type robot tractor developed by Vehicle Robotics Laboratory (VeBots) of Hokkaido University in Japan. It could autonomously perform various farm works like seeding, tillage, cultivating, etc. The steering, engine rotation, vehicle speed, PTO, and Hitch can be controlled by a robot controller embedded inside the tractor.

Figure 1.1 A robot tractor developed by VeBots Lab. in Japan.

Generally, agricultural autonomous vehicles are divided into two categories, one kind is used for an open field and the other kind is used for indoors. Usually, vehicles used for an open field are applied to harvesting, tillage, fertilizing, spraying, cultivating, transportation (Chateau *et al*., 2000; Bell, 1999; Fehr *et al*., 1995; Noguchi, 1998; Reid

& Searcy, 1987; Stombaugh *et al*., 1998). Orchard vehicles are also categorized into the open field application. However, it should be treated in a different way as the orchard environment different from a paddy field or wheat field because the canopy can block Global Positioning System (GPS) signals (Barawid *et al*., 2007). Indoor use of autonomous vehicles is involved mainly in greenhouse works. And those vehicles are navigated mainly using machine vision and dead reckoning rather than GPS (Yin *et al.,* 2013).

### 1.1.2 GPS based guidance system

Since early 1990s, a GPS receiver has been widely used as global guidance sensor (Bell, 2000; Larsen *et al*., 1994; Yukumoto *et al*., 2000). A GPS based guidance system can be used for many field operations such as tillage, planting, cultivating, and harvesting.

Some agricultural machinery companies and GPS companies have made guidance systems (Trimble Co. Ltd., 2013, Topcon Co. Ltd., 2013). These systems use a GPS and an inertial measurement unit (IMU) to locate the position and orientation of a vehicle. A computer calculates displacement from a formally planned path, and guides the operator to steer the wheel automatically. Figure 1.2 shows a GreenStar 3 2630 guidance user interface of John Dreere Co. Ltd. The touch screen unit can interface with global positioning satellites to allow farmers to track what is being planted and how much fertilizer is going in the ground and where.

However, the high cost of precision GPS receivers is the major obstacle for their widespread use in agricultural vehicle navigation.

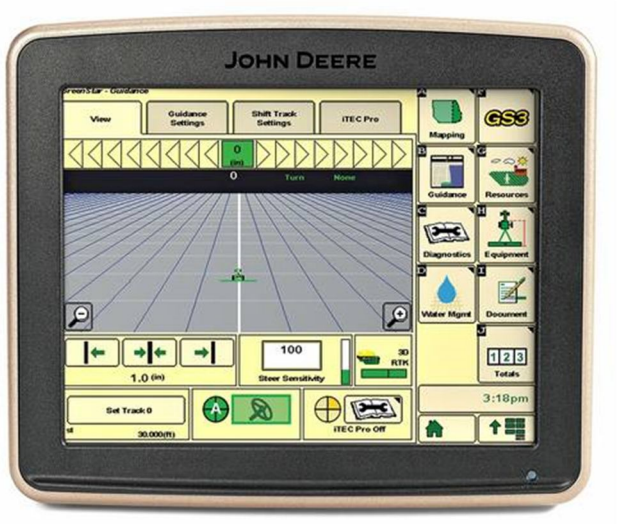


Figure 1.2 Greenstar 3 2630 guidance system of John deere Co. Ltd.

### 1.1.3 Machine vision based guidance system

A machine vision was used early from 1980's, when the PC became compact and price acceptable. Machine vision technology can be used to automatically guide a vehicle when crop row structure is distinguishable in a field. Typical applications include guiding a tractor for crop row cultivation (Han. S. *et al*., 2004), or guiding a combine for harvest operation (Benson. E.R. *et al*., 2003). The guidance sensor, i.e., the camera, is a local sensor because only the relative location of the vehicle, with respect to the crop rows, can be determined. Machine vision guidance has the advantage of using local features to fine-tune the vehicle navigation course. It has the technological characteristics closely resembling those possessed by a human operator, and thus has great potential for implementation of a vehicle guidance system (Wilson, 2000).

In a machine vision based guidance system, finding guidance information from crop row structure is the key in achieving accurate control of the vehicle. A number of image processing techniques have been investigated to find the guidance course (or directrix) from crop row images. As examples, Reid *et al*. (1985) developed a binary threshold

strategy using a Bayes classification technique to segment crop canopy and soil background for cotton crop effectively and accurately at different growth stages. Gerrish *et al*. (1985) concluded in their study that threshold intensity images alone will not work in all cases, and they showed that the combination of noise filtering, edge detection, threshold, and re-scaling was the most promise technique. Image analysis using Hough transform to find crop rows was also reported in several studies (Marchant and Brivot, 1995; Marchant, 1996). Another crop row detection method was proposed by Olsen (1995) without depending on the segmentation of the crop rows. Olsen used a low-pass filter to process the pixel's grey value sum-curve to find the offset as shown in Figure 1.3. In addition, a band-pass filter-based approach to crop row detection and tracking was developed by Hague and Tillett (2001).

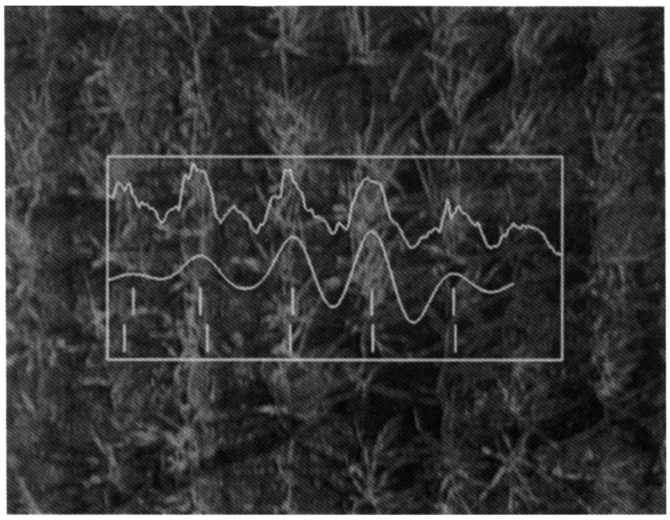

Figure 1.3 Crop rows finding by means of a low-pass filtering process. (Olsen, 1995).

### 1.1.4 Laser scanner based guidance system

Gordon and Holmes (1988) developed a custom built laser scanner system to continuously monitor a moving vehicle's position. Carmer and Peterson (1996) discussed the use of laser scanner for various applications in robotics, such as for ranging and obstacle avoidance. Ahamed *et al*. (2004) used a laser scanner for developing a positioning method using reflectors for infield road navigation. They tested differently shaped reflectors to determine the accuracy in positioning. Laser scanner has been used for navigating a small vehicle through an orchard (Tsubota *et al*., 2004). A guidance system using laser scanner was found to be more stable than using a GPS in a citrus orchard setting (Subramanian *et al*., 2006). Barawid *et al*. (2007) developed an autonomous navigation system using a two-dimensional (2D) laser in an orchard application. In this system a line detection algorithm based on Hough transform was adopted to recognize the tree rows so that the vehicle could travel through the orchard without collisions. The Carnegie Mellon University has used a 3D scanning laser rangefinder within the framework of its NavLab project (Thorpe, 1990).

## 1.2 Research motivation and objectives

Driving an agricultural vehicle straight for hundreds of meters in a large field is a boring and easy tired task. A nighttime farming has various merits other than increasing the machine operating time. At night, lower temperature and absence of sunlight can reduce fatigue in farmers and can also minimize pesticide drift owing to less wind. But it is difficult for a driver to operate as accurate as the daytime. In addition, it is reported that nighttime plowing decreases weed germination (Buhler, 1997; Hartmann and Nezadal, 1990).

Various guidance systems have been developed and are available in the market to assist the operator driving at daytime and night by showing current vehicle direction and position as well as working path. However, at present, the guidance image displayed on the terminal is an unrealistic computer-generated image (CGI) and does not project the surroundings realistically. In an actual environment, encountering unexpected obstacles is quite possible. Hence, if an actual image is overlapped on the navigation image, it will be more intuitive and easier to perceive.

The technique that blends computer graphics (virtual reality) with the real-world environment in real time is called augmented reality (AR) or mixed reality (MR) (Furht, 2011). In this technique, text or objects are drawn on an actual image to help people understand reality. A common example of AR occurs in sports programs on television. A computer-generated topographical mesh is drawn on the putting green in a golf program, or virtual advertisements are displayed on an actual wall of a baseball or football stadium. In addition, AR is used in many other areas such as military, aerospace, video games, surgery (Liao *et al*., 2010), and machine maintenance. Recently, AR has been applied to a parking assist system for automobiles.

In this thesis, three main objectives were aimed to be achieved. The first objective was to develop a guidance system for a mostly used agricultural vehicle - tractor. The second objective was to develop a guidance system for a universal combine harvester that can be used for wheat, rice and soybean harvesting. In addition, the second guidance system was aimed to be used for auto guidance for the combine harvester.

The first guidance system was going to use the AR technology to create virtual guidance information merged with a real environment image from a vehicle camera. To achieve this objective, the following issues were considered:

1) The lens distortion of the camera used for this study was calibrated. And the posture relationship of the camera to the tractor was calibrated also.
2) Matching of GPS data with the image from the camera.
3) A method to detect edge of a road where the tractor was running and a method to show the edge to the image of the camera was considered.

The second guidance system was aimed to be used for a soybean harvesting environment using a laser scanner. The reason why we used a laser scanner in this study was that the laser scanner was a self-contained active sensor, which does not rely on outside illumination. To achieve this objective, we were going to do:

1) Developing a soybean detection algorithm that can segment field and soybean crops.
2) Generating a guidance line from the position information of the detected crops.
3) Calculating guidance parameters from the current vehicle position and direction with relative to the detected guidance line.

The third objective was going to use the guidance system based on laser scanner. In detail we were going to achieve:

1) Calculating a steering value based on the guidance parameters that calculated by the laser scanner based guidance system.
2) Trying to control the combine harvester following a crop row of soybean.
3) Evaluating accuracy of the developed auto guidance system using an RTK-GPS.

# CHAPTER 2

# RESEARCH PLATFORM AND SENSORS

## 2.1 Research platform

This chapter introduces the information of the tractor and combine harvester platform and specifications of the sensors used in this study.

Tractor guidance system using AR (augmented reality) provides tractor direction or a dangerous position in the field and agricultural road. Tractor guidance system used camera, GPS and IMU. Camera used to make a real image. Two RTK-GPS were used to measure the yaw angle and position of the tractor. An IMU determined the roll and pitch angles.

Combine harvester guidance system acquired edge information from laser scanner and pan tilt unit. Laser scanner was measured distance between combine harvester and crop rows. Pan tilt unit was used to tilt the laser scanner up and down.

### 2.1.1 Tractor

The tractor platform of this study was a 56 kW commercial wheel type tractor (MD77, KUBOTA Co., Ltd., Japan) as shown in Figure 2.1. The specifications of the tractor are given in Table 2.1. In this platform was modified by installing a camera and a GPS guidance system.

Figure 2.1 Experiment platform Kubota MD77.

**Table 2.1 Specifications of the tractor.**

| | | |
|---|---|---|
| Model | KUBOTA MD77 | |
| Drive Function | 4 Wheel Drive | |
| Size | Height (mm) | 2590 |
| | Width (mm) | 1855 |
| | Length (mm) | 3880 |
| Weight (kg) | | 3200 |
| Engine | Model | KUBOTA V4302-L |
| | Power(kW) | 56 |

The overall architecture of chapter 3 tractor guidance system is shown in Figure 2.2. There are three sensors of the tractor guidance system: GPS1, GPS2, camera and IMU. Two GPSs and IMU interface was used RS-232C. The camera interface was used IEEE 1394.

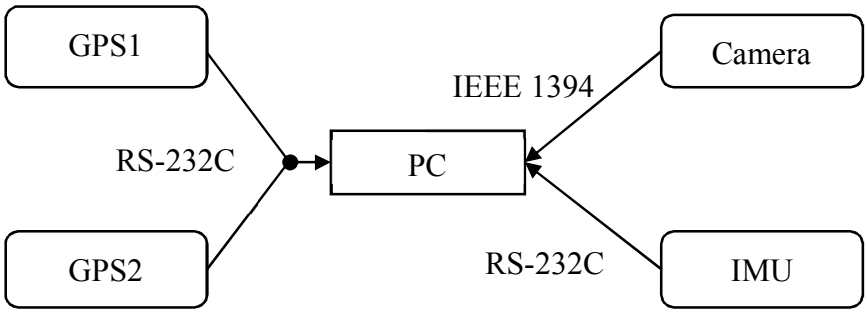


Figure 2.2 Overall system architecture of the tractor guidance system.

### 2.1.2 Combine harvester

Indicated in Figure 2.3 is the platform on which the experiments were conducted, AG1100 Combine Harvester of YANMAR Co., Ltd. This combine harvester can work in both "Manual Mode" and "Automatic Mode", in automatic mode, the driving part can be controlled by the robot, including going forward and back, steering left or right or any combination of these operations. Safety of this combine harvester has been improved that in Automatic Mode, driving commands should be sent to the combine within every 200 milliseconds; otherwise the combine will stop and sound an alarm.


Figure 2.3 Combine harvester platform (YANMAR AG1100).

The overall architecture of chapter 4 and 5 combine harvester guidance system is shown in Figure 2.4. There are two main sub-systems of the combine harvester guidance system: Control PC of the combine harvester, Crop rows detected system.

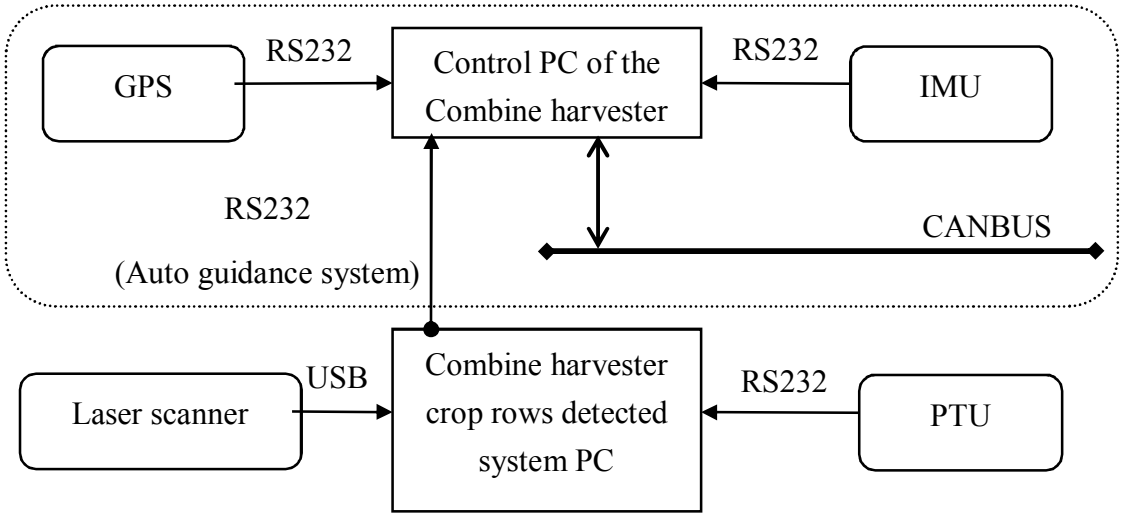


Figure 2.4 Overall system architecture of the combine harvester guidance system.

## 2.2 Global navigation sensors

### 2.2.1 RTK-GPS

The Global Positioning System (GPS) is a worldwide radio-navigation system that consists of a constellation of 24 or more satellites, a number of ground stations, and millions of users. The GPS was developed by the U.S. Department of Defense starting in the 1970s as a military system (Parkinson and Spilker, 1996). GPS technology delivers a range of benefits and advantages to growers. As global markets become more competitive and an increasingly populated world reduces available farm land, GPS guidance is now being relied upon to drive productivity and efficiencies in agriculture from ground preparation to fertilizer application, planting, spraying and harvesting. During the early years of GPS, the Department of Defense intentionally degraded the

quality and accuracy of Navstar GPS signals in the interest of national security through a process known as "selective availability". However, in May of 2000, a presidential executive order ended such degradation of GPS signals in order to make more widespread use of GPS practical for civilian use. This action allowed up to 10 times improved accuracy for civilian GPS receivers, including those used in agriculture (Buick, 2006).

To produce a GPS position, a GPS receiver receives signals from a minimum of four satellites. These GPS signals from the satellites are collected by an antenna, amplified, and converted to digital timing signals and satellite orbital data that are used to calculate the user's position. The accuracy of GPS is affected by a number of error sources. Some of these errors are correctable by the use of differential GPS (DGPS), while other errors are not correctable. The most important uncorrectable error sources of GPS are caused by the receiver and antenna design, and multipath interference in the user's local environment. The most important DGPS-correctable errors are ionosphere-induced signal distortions, satellite timing errors, and satellite ephemeris errors. GPS errors also depend on the method of differential correction. The relative errors of a GPS generally grow with the time of observation (Jorge and Arthur, 2009).

DGPS (Differential GPS) receivers use a second signal and can position within 1 m. The most accurate GPS receivers using a technique called real-time kinematic (RTK) positioning that can position within a few centimeters. In this research, RTK-GPS used measure the yaw angle and position of the tractor. In chapter 4 and 5, RTK-GPS used measure the combine harvester position and reference path of soybean rows.

For the dedicated RTK shown in Figure 2.5 (a), a GPS receiver (Topcon Legacy-E, specification shown in Table 2.2) was attached to the vehicle as the rover station and another GPS receiver (Trimble MS750, its specification shown in Table 2.3) was set up

on the building roof as the base station. For correction signal transmission, two small-area wireless communication transceivers were connected through RS232C to the base station as the transmitter and the rover station as the receiver, respectively. One disadvantage of the base station RTK was that the correction data would get unstable in case of obstructions between the user and the base station like high buildings or trees, which limited the user into a certain area.

For the VRS-RTK configuration shown in Figure 2.5 (b), the RTK VRS network was used instead of the dedicated based station mentioned above and the correction signal was obtained via a PDA (Personal Digital Assistant) through which the GPS service was provided in Japan. Compared with the base station RTK, the VRS RTK was more stable and allowed for more freedom of movement without the need to switch based stations.

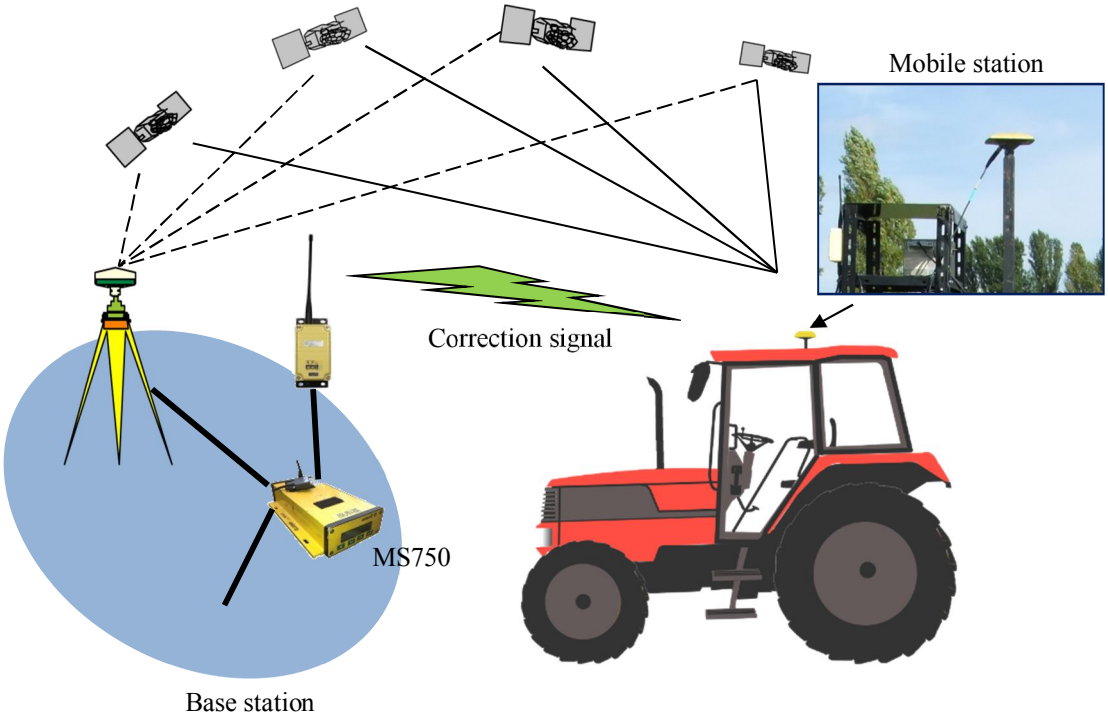


(a) Dedicated RTK set up in Hokkaido University.

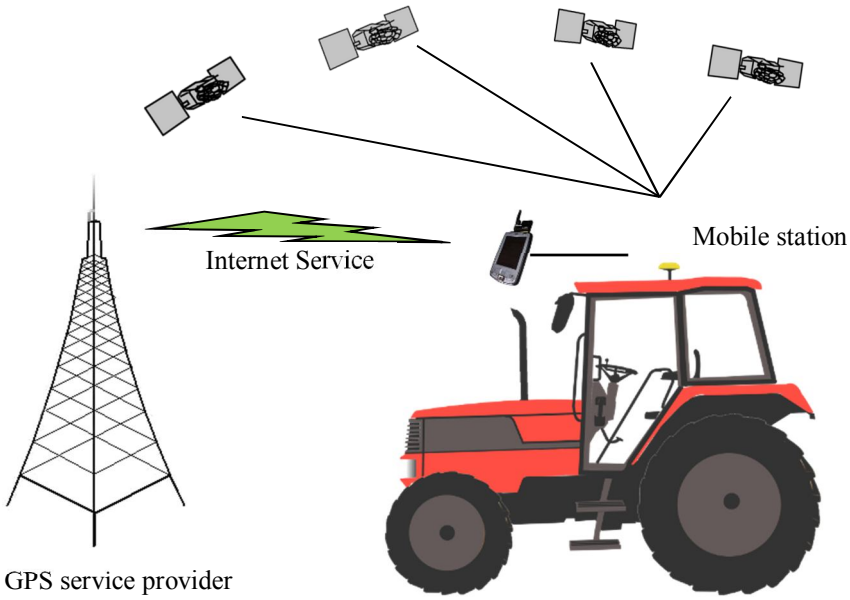


(b) Virtual Reference System (VRS) RTK via a cell phone network in Japan.

Figure 2.5 RTK-GPS solutions.

In this research, the RTK-GPS receivers were also used together with other sensors like IMU to evaluate the accuracy along predetermined paths in guidance system and to evaluate the performance of the auto guidance system.

**Table 2.2 Technical specifications of Topcon Legacy-E.**

| | |
|---|---|
| **Legacy-E**: *40 channel integrated GPS+ receiver with MINTER interface.* | |
| **Technical specifications:** | |
| Tracking channel, standard | 40 L1 GPS (20 GPS L1+L2+GLONASS on Cinderella[2] days) |
| Tracking channel, optional | 20 GPS L1+L2 (GD), 20 GPS L1+GLONASS (GG)<br>20 GPS L1+L2+GLONASS (GGD) |
| Signal Tracked | L1/L2 C/A and P Code & Carrier |
| Baseline Accuracy | 5mm+0.5ppm |
| RTK (OTF) Accuracy | 10mm+1ppm |
| Radio | |
| Type | External, UHF/VHF radio modem |
| Base Power Output | 0.5W/2.0W/35W |
| **Physical characteristics:** | |
| Size | 24 cm W × 11cm H × 3.5 cm D |
| Weight | 0.6 kg (1.32 lbs) |
| Power | 6 to 28 volts DC, less than 3.3 Watts |

**Table 2.3 Technical specifications of Trimble MS750.**

| **MS 750**: *Dual Frequency RTK Receiver for Precise Dynamic Positioning.* | |
|---|---|
| **Technical specifications:** | |
| Tracking | 9 channels L1 C/A code, L1/L2 full cycle carrier<br>Fully operational during P-code encryption |
| Signal processing | Supertrak Multicity Technology/Everest Multipath Suppression |
| Positioning mode | |
| Synchronized RTK | accuracy, 1 cm + 2ppm Horizontal, 2 cm + 2 ppm Vertical<br>max. output rate, 300 ms<br>max rate, 5 Hz Std. |
| Low output rate | accuracy, 2 cm + 2ppm Horizontal, 2 cm + 2 ppm Vertical<br>max. output rate, <20 ms<br>max rate, 20 Hz |
| DGPS | accuracy, <1m<br>max. output rate, <20 ms<br>max rate, 20 Hz |
| Range | Up to 20 km from base for RTK |
| **Physical characteristics:** | |
| Size | 14.5 cm W × 5.1 cm H × 23.9 cm D |
| Weight | 1.0 kg (2.25 lbs) |
| Power | 12 VDC / 24 VDC, 9 Watts |

## 2.3 Localization navigation sensors

### 2.3.1 Inertial measurement unit

In guidance system, the vehicle's attitude including its heading direction needs to be measured in determination of its heading angle and location. Figure 2.6 shows angle

definition in roll, pitch and yaw. Considering degradation of GPS signal by obstruction, the GPS antenna is always fixed at a higher level over the center of gravity (CG) of vehicles, resulting in that the antenna shifts from the vehicle's CG on the ground level because of inclinations including roll and pitch directions as shown in Figure 2.7. Therefore, inclinations need to be measured in order to calculate the vehicle's actual position other than using the GPS antenna's position directly.

In this research, an inertial measurement unit (IMU, JCS-7402 shown in Figure 2.8) was used to measurement the vehicle's attitude, angles in Roll, Pitch and Yaw, in real-time. Table 2.4 shows the specifications of JCS-7402. The IMU could measure the angular velocity within the range of 100°/s. It also could measure roll and pitch angles within the range of 45°, and yaw angle of 180°. Its drift rate was specified as 0.5°/hr. It had the capability of outputting digital signals with resolutions 0.1°. The digital output signal was transmitted to the vehicle computer at a frequency of 50 Hz/200 Hz through a RS232C serial port.

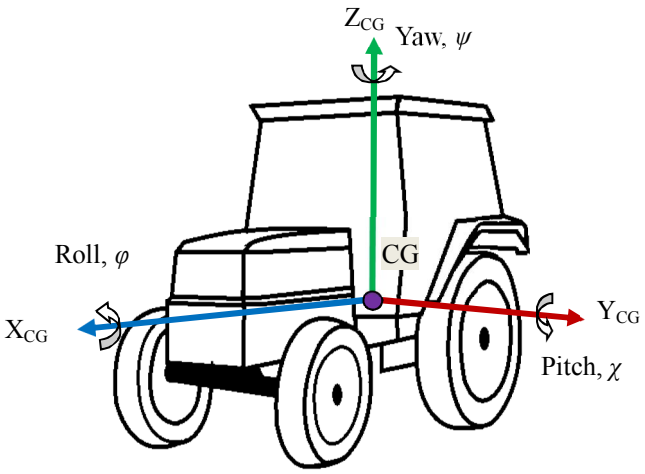


Figure 2.6 Definition of roll, pitch and yaw of the vehicle.

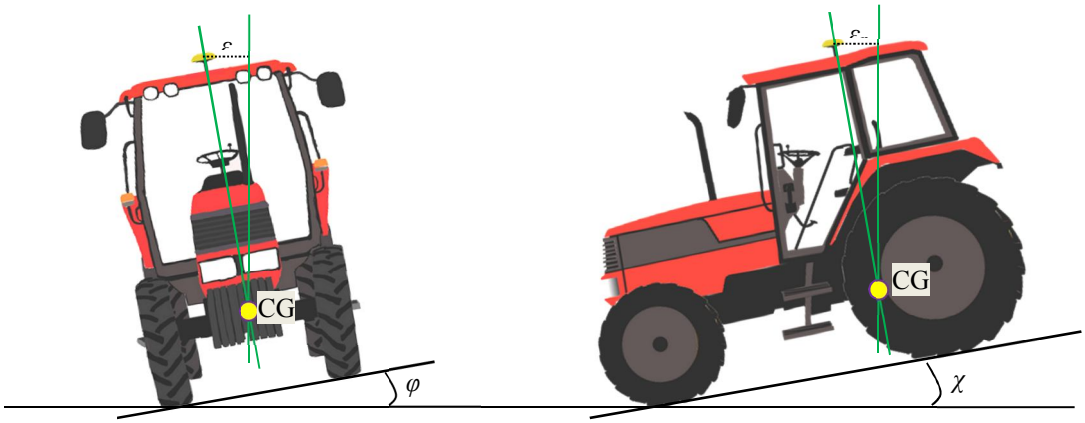


Figure 2.7 Inclinations in pitch and roll.

**Table 2.4 JCS-7402 Specifications**

| | | |
|---|---|---|
| **JCS7402**: *FOG attitude measurement system.* | | |
| **Digital characteristics (RS232, RS422):** | | |
| Output | Baud Rate | 19.2Kbps/115.2Kbps |
| | Frequency | 50Hz/200Hz |
| Measurement | Roll angle | ±45° |
| | Pitch angle | ±45° |
| | Relative heading angle | ±180° |
| | Rate (X, Y, Z) | ±100°/s Max |
| | Acceleration (X, Y, Z) | ±19.6 $m/s^2$ Max |
| Resolution | Angle | 0.1° Max |
| | Rate | 0.1°/s Max |
| | Acceleration | 0.1 $m/s^2$ Max |
| **Power supply:** | | |
| Input power | | +20~ +30 VDC |
| Current | | <1.0 A |
| **Dimensions:** | | |
| L × W × H | | 170 × 170 × 141 mm |

Figure 2.8 IMU for attitude measurement.

Since it measures the relative heading angle with a high accuracy, the IMU is usually integrated with the RTK-GPS mentioned above using fusion algorithms to acquire the absolute heading of the vehicle. Noguchi *et al*. (1998) developed a guidance system by integrating RTK-GPS and GDS using the EKF algorithm to reach a higher accuracy with the lateral error of about 8.4 cm compared with the RTK-GPS error of 20 cm.

### 2.3.2 CCD camera

In chapter 3, IEEE 1394 digital color camera (SONY DFW-VL500) was adapted in navigation sensor. CCD camera is shown in Figure 2.9. It was mounted on an aluminum frame on the tractor roof. The camera was inclined forward. A wide conversion lens was attached on the camera to broaden the field of view. The camera interface was IEEE 1394, which allowed the camera settings to be controlled programmatically from a computer.

Table 2.5 shows the specifications of DFW-VL500 CCD camera. The DFW-VL500 is a fully digital camera which adopts the IEEE1394-1995 standard. Cameras incorporate the latest 400 Mbps chip set and feature Sony's W-fine CCD which integrates a primary color filter ensuring high color accuracy square pixels and Progressive Scan technology which provides sharp, high resolution images, even of fast moving objects. Also, both models include an external trigger mode for asynchronous trigger operation that

provides jitter-free pictures since the camera acquisition can be synchronized to full random events.

Through the IEEE1394-1995 high performance serial bus, the DFW-V500/VL500 presents 30 fps in VGA (640×480) resolution format. The DFW-V500 has a C type lens mount while the DFW-VL500 includes a 12× zoom lens with motorized zoom, iris and focus. A latching 6-pin IEEE1394 connector is used to output the digital image, to power the camera and to control all functions of the camera through a computer.

**Table 2.5 Specifications of DFW-VL500 CCD camera**

| **DFW-VL500**: *IEEE 1394 digital color camera.* | |
|---|---|
| **Interface format (IEEE1394):** | |
| Data format | 640×480 YUV(4:2:2) 8bit 320×240 YUV(4:2:2) 8bit<br>640×480 YUV(4:1:1) 8bit 160×120 YUV(4:2:2) 8bit |
| Frame Rate | 3.75, 7.5, 15.0, 30 fps and one shot |
| Image device | 1/3" Wfine CCD |
| White balance | ATW, One push, 3200°k, 5600°k, Manual |
| Shutter speed | 5~1/15, 1/30~1/100000 sec. |
| Gain | Automatic and manual control |
| Power | Supplied through IEEE 1394 cable(8 to 30vdc), 4W |
| Weight | 335g |
| Lens control | 12×zoom lens, automatic and manual |

Figure 2.9 DFW-VL500 digital CCD camera.

### 2.3.3 2D laser scanner

In chapter 4 and 5, the navigation sensor was a 2D laser scanner (UTM-30LX, Hokuyo, Japan), which was mounted on the front of the combine harvester. Figure 2.10 shows the 2D laser scanner. The 2D laser scanner is a scanning laser scanner with an extended sensing range out to 30 meters. Interface to the sensor is through USB 2.0 with an additional synchronous data line to indicate a full sweep. Scanning rate is 25 milliseconds across a 270° range. A 12V power source is required. The distance error of the laser scanner is ±5cm. A two-dimensional laser scanner was used as the primary navigation sensor to detect the crop rows. Table 2.6 shows the specifications of 2D laser scanner. This laser scanner employs a laser optical scanner to detect the distance of an object of interest by measuring the "time-of-flight" of laser light pulses.

Figure 2.10 2D Laser scanner (UTM-30LX).

**Table 2.6 Specifications of a 2D laser scanner(UTM-30LX).**

| | |
|---|---|
| Power source | Voltage: 12 VDC±10%<br>Current: Max:1A, Normal: 0.7 A |
| Light source | Semiconductor laser diode (λ=905nm)<br>Laser safety Class 1 (FDA) |
| Detection range | 0.1 to 30m (White square kent sheet 500 mm or more)<br>Max.60 m (<30 m guaranteed) |
| Scan angle | 270° |
| Accuracy | 0.1 to 10 m: ±30 mm<br>10 to 30 m: ±50 mm |
| Angular resolution | 0.25°(360°/1,440 steps) |
| Scan time | 25 msec/scan (40 Hz) |
| Sound level | Less than 25dB |
| Interface | USB2.0 (Full Speed) |
| Synchronous output | NPN open collector |
| Command system | Exclusively designed command SCIP Ver.2.0 |
| Connection | Power and Synchronous output: 2 m flying lead wire<br>USB: 2m cable with type-A connector |
| Amblent<br>(Temperature/Humidity) | -10 to +50 degrees C<br>less than 85% RH (without dew and frost) |
| Vibration resistance | Double amplitude 1.5 mm 10 to 55 Hz, 2 hours each in X, Y and Z direction |
| Impact resistance | 196 $m/s^2$, 10 times in X, Y and Z direction |
| Weight | Approx. 370g (with cable attachment) |

### 2.3.4 Pan tilt unit

In chapter 4 and 5, a pan-tilt unit (PTU-D46, Directed Perception, Inc.) was adopted on combine harvester. Figure 2.11 shows PTU-46. The PTU-D46 family of miniature pan-tilt units provides fast, precise positioning in an extremely small and lightweight package. They are fully computer-controlled and offer programmability of speed, acceleration, power, and other parameters.

The included controller, with built-in RS-232C and RS-485 interfaces, handles precise kinematic motion control according to user-set parameters. The PTU-D46 units accept ASCII and binary command formats and is networkable. Table 2.7 presents its specifications. This Pan/Tilt Unit provides rotations in both pan and tilt directions with a high resolution and can be controlled easily by computers via RS-232C.

Figure 2.11 Pan tilt unit (PTU-D46-17).

**Table 2.7 PTU-D46 Specifications.**

| **PTU-D46**: Miniature computer-controlled pan-tilt unit. | |
|---|---|
| **Technical specifications:** | |
| Rated payload | 2.72kg |
| Unloaded speed | 300°/s Max @30VDC |
| Resolution | 0.013° |
| Tilt range | -47° to +31° |
| Pan range | -159° to +159° |
| Power requirements: | |
| Input voltage | 12-30 VDC unregulated |
| Power consumption | 13 watts for full power mode at 30 VDC |
| **Connections & communications:** | |
| Host interface | RS-232 (DB-9 female connector), RS-422/-485 |
| Control protocols | DP (ASCII, Binary) |
| Mechanical: | |
| PTU weight | 3lb |
| Dimensions | 3”(H) × 5.13”(W) × 4.25'(D) |

# CHAPTER 3

# GUIDANCE SYSTEM USING A CAMERA AND GPS FOR A TRACTOR

## 3.1 Introduction

This chapter introduces a tractor guidance system using an augmented reality (AR). The guidance system used GPS, IMU, PC, a camera for tractor guidance. In section 3.2, two GPSs, camera and IMU was mounted at the roof of a tractor will be introduced. Two GPS was utilized in this study to measure the yaw angle and position of the tractor. An IMU determined the roll and pitch angles. Mixing a computer generated 3D model with an actual video image in real time. Also, the lens distortion of the camera was calibrated. And the posture relationship of the camera to the tractor was calibrated. In section 3.3, result of the camera calibration will be discussed. Section 3.4 gives the conclusion of this chapter.

## 3.2 Materials and methods

### 3.2.1 Tractor guidance system

Figure 3.1 shows a schematic of the tractor guidance system. First, a three-dimensional (3D) model was developed by surveillance using a real-time kinematic GPS (RTK-GPS). The 3D coordinates of the corners of the field, edges of the road, and other objects were

located. This allows any landmark to be included in the model. Next, paths were generated at regular intervals. These processes were completed before actual operation of the tractor on the field. Two RTK-GPSes (Trimble MS 750) were used to measure the yaw angle and position of the tractor. An IMU determined the roll and pitch angles. From these data, the position and orientation of the actual camera were estimated. A virtual camera was positioned at exactly the same coordinates as those of the actual camera. From that viewpoint, the points and lines in a 3D model projected on an image plane should be matched with the actual landmarks in an image taken by the actual camera. Since the image taken by the actual camera was distorted due to the characteristics of the lens, it was rectified and then mixed with the virtual perspective image. The resulting image is called the AR image. In this image, a path and other objects are drawn on the real field image. The operator watches the display while driving the tractor.

Figure 3.3 shows an example of the AR image created in this chapter. A 3D model shows the left and right sides of the farm road. This model is recorded as a sequence of 3D coordinates. Looking from the point indicated by a yellow arrow in Figure 3.3 (a), the 3D model appears as a virtual perspective image in Figure 3.3 (b), while the actual image appears in Figure 3.3 (c). The synthesized image (Figure 3.3 (d)) shows the edge of the road and an unseen bridge.

Figure 3.2 shows a tractor equipped with the AR guidance system, which includes GPS antennae, an IMU, a PC, and an IEEE 1394 digital color camera (SONY DFW-VL500). They were mounted on an aluminum frame on the tractor roof. The camera was inclined forward. A wide conversion lens was attached on the camera to broaden the field of view.

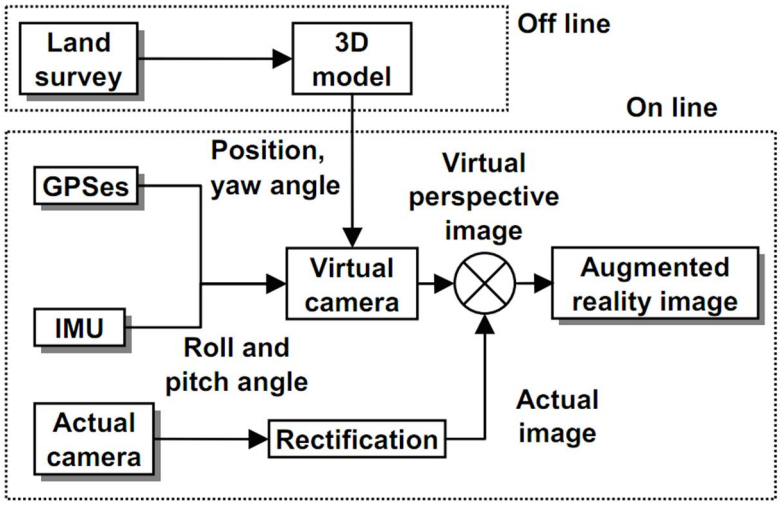


Figure 3.1 Schematic of the tractor guidance system.

The camera interface was IEEE 1394, which allowed the camera settings to be controlled programmatically from a computer. National Instruments LabVIEW 8.5 was used for programming. For the subroutines that required much calculation, Microsoft Visual Studio 2008 was used to make a dynamic link library (DLL). The resolution of the image was 640 pixels × 480 pixels. The refresh frequency of the AR image was 30 Hz. This frequency was restricted by the camera. A monitor was placed in front of the steering wheel. The time taken from image capturing to displaying was within 10 ms.

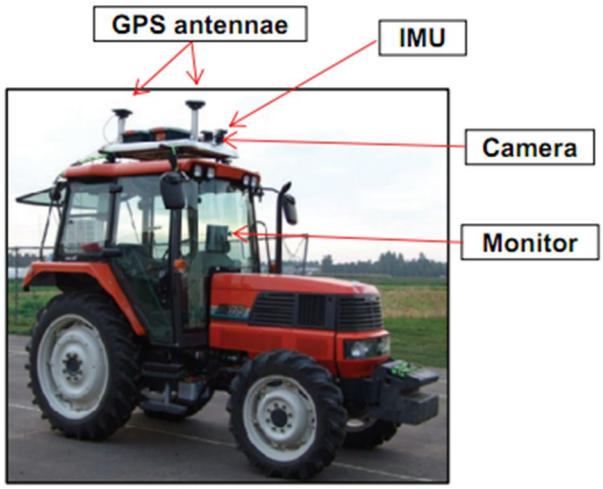


Figure 3.2 AR tractor guidance system.

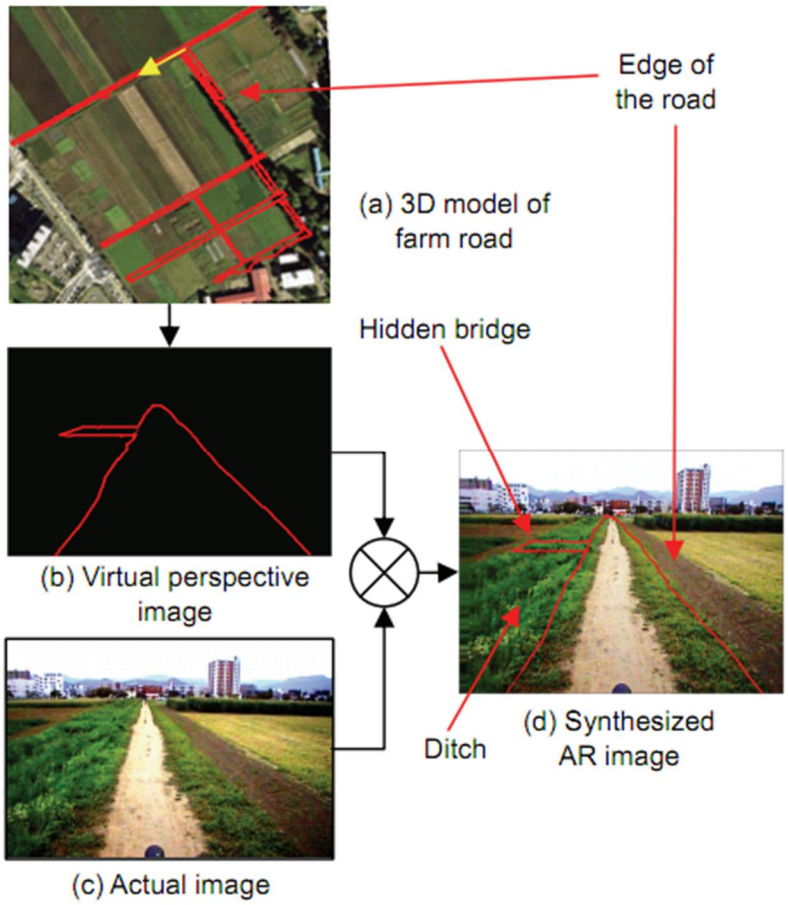


Figure 3.3 Example of the AR image.

### 3.2.2 Definition of frames of reference for the tractor guidance system

In this system, frames of reference were defined as shown in Figure 3.4. The universal transverse mercator (UTM) system was used for the world coordinates $X_w$ - $Y_w$ - $Z_w$. Its $X_w$, $Y_w$, and $Z_w$ axes are the easting, northing, and altitude of the UTM, respectively. The origin of the reference frame of the tractor was set at the point right under the center of the rear axle. The positions of the tractor $(X_{wt}, Y_{wt}, Z_{wt})^T$ and the camera $(X_{wc}, Y_{wc}, Z_{wc})^T$ in the world reference frame were defined as follows:

$$\begin{bmatrix} X_{wt} \\ Y_{wt} \\ Z_{wt} \end{bmatrix} = \begin{bmatrix} X_{wGPS1} \\ Y_{wGPS1} \\ Z_{wGPS1} \end{bmatrix} + E_{x180} E_{z\psi} E_{wt} \begin{bmatrix} x_{tGPS1} \\ y_{tGPS1} \\ z_{tGPS1} \end{bmatrix} \tag{3-1}$$

$$\begin{bmatrix} X_{wc} \\ Y_{wc} \\ Z_{wc} \end{bmatrix} = \begin{bmatrix} X_{wGPS1} \\ Y_{wGPS1} \\ Z_{wGPS1} \end{bmatrix} + E_{x180} E_{z\psi} E_{wt} \begin{bmatrix} x_{cGPS1} \\ y_{cGPS1} \\ z_{cGPS1} \end{bmatrix} \tag{3-2}$$

$$E_{x180} = \begin{bmatrix} 1 & 0 & 0 \\ 0 & \cos 180° & -\sin 180° \\ 0 & \sin 180° & \cos 180° \end{bmatrix} = \begin{bmatrix} 1 & 0 & 0 \\ 0 & -1 & 0 \\ 0 & 0 & -1 \end{bmatrix} \tag{3-3}$$

$$E_{z\psi} = \begin{bmatrix} \cos\psi & -\sin\psi & 0 \\ \sin\psi & \cos\psi & 0 \\ 0 & 0 & 1 \end{bmatrix} \tag{3-4}$$

$$E_{wt} = E_{IMU} (E_{IMUini})^{-1} \tag{3-5}$$

$$E_{IMU} = \begin{bmatrix} \cos\rho & 0 & \sin\rho \\ 0 & 1 & 0 \\ -\sin\rho & 0 & \cos\rho \end{bmatrix} \begin{bmatrix} 1 & 0 & 0 \\ 0 & \cos\theta & -\sin\theta \\ 0 & \sin\theta & \cos\theta \end{bmatrix} \tag{3-6}$$

$$E_{IMUini} = \begin{bmatrix} \cos\rho_{ini} & 0 & \sin\rho_{ini} \\ 0 & 1 & 0 \\ -\sin\rho_{ini} & 0 & \cos\rho_{ini} \end{bmatrix} \begin{bmatrix} 1 & 0 & 0 \\ 0 & \cos\theta_{ini} & -\sin\theta_{ini} \\ 0 & \sin\theta_{ini} & \cos\theta_{ini} \end{bmatrix} \tag{3-7}$$

Here $(X_{wGPS1}, Y_{wGPS1}, Z_{wGPS1})^T$ is the coordinate of GPS1 in the world reference frame. $(x_{tGPS1}, y_{tGPS1}, z_{tGPS1})^T$ and $(x_{cGPS1}, y_{cGPS1}, z_{cGPS1})^T$ are the initial

coordinates of the tractor origin and the camera origin, respectively, as viewed from GPS1. $E_{x180}$ is a rotation matrix around X axis for 180°. $E_{z\psi}$ is a rotation matrix around Z axis for an angle $\psi$. $E_{wt}$, $E_{IMU}$, and $E_{IMUini}$ are the frames of reference of the tractor, the IMU, and the initial condition of the IMU, respectively. $\psi$ is the yaw angle calculated from the relative positions of GPS1 and GPS2 (Alkan and Baykal, 2001). $\theta_t$ and $\rho_t$ are the roll and pitch angles measured by the IMU, respectively. $\theta_{ini}$ and $\rho_{ini}$ are the roll and pitch angles of the IMU when the tractor is put on a flat surface. The initial parameters of the IMU were measured simultaneously with the extrinsic parameters of the camera.

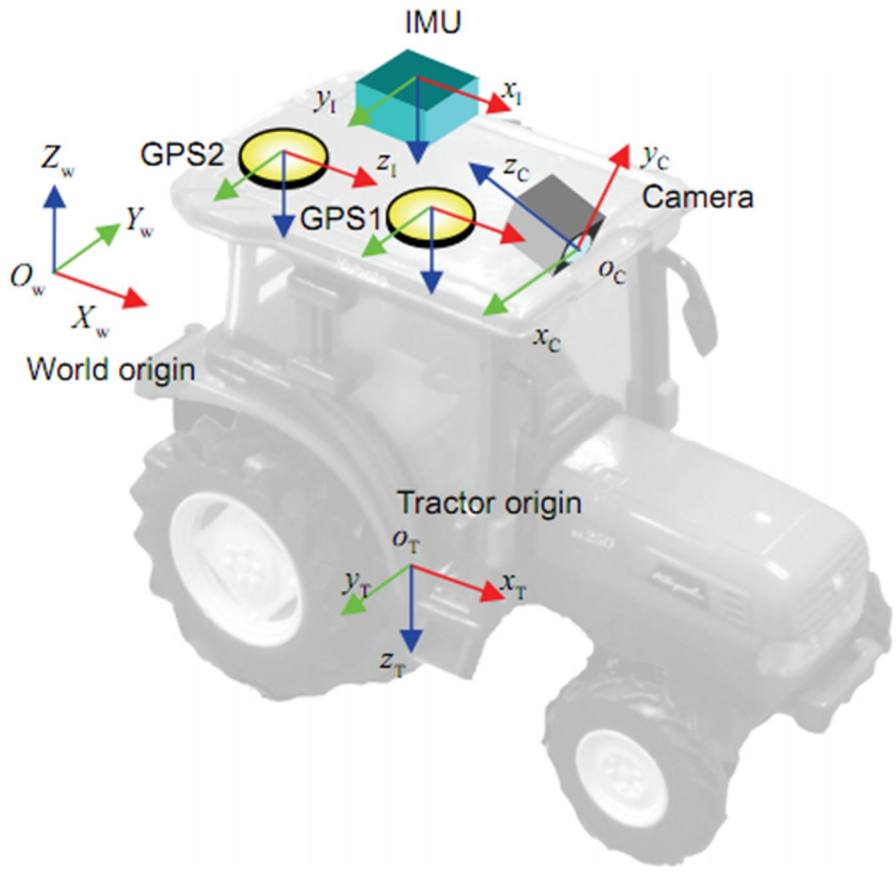


Figure 3.4 Frames of reference of the system.

### 3.2.3 Camera calibration

To match the virtual image with the actual image, the intrinsic parameters (focal length, image center, and lens distortion coefficients) and the extrinsic parameters (position and orientation of the camera) were estimated using the camera calibration method.

(1) Estimation of the camera's intrinsic parameters

Unlike the image taken by an ideal virtual camera, the actual image includes distortion and the offset of principal points. The intrinsic parameters (focal length, principal point position, and lens distortion) of the camera must be known. To estimate the intrinsic parameters, commercial photogrammetric software Photo Modeler 6.0, from Eos Systems, was used. The images of a company-distributed test grid pattern were taken from 12 different directions according to the instructions of the software. The parameters were calculated automatically. As shown in Figure 3.5, defining the coordinates in distorted image $(x_d, y_d)^T$ rectified image $(x_T, y_T)^T$ and defining principal point $(P_x, P_y)^T$, rectification was performed with the following equations (EOS Systems Inc., 2007):

$$\begin{bmatrix} x_r \\ y_r \end{bmatrix} = (1 + d_r) \begin{bmatrix} x_d - P_x \\ y_d - P_y \end{bmatrix} \tag{3-8}$$

$$d_r = K_1 r^2 + K_2 r^4 + K_3 r^6 \tag{3-9}$$

$$r^2 = (x_d - P_x)^2 + (y_d - P_y)^2 \tag{3-10}$$

where $K_1$, $K_2$, and $K_3$ are distortion constants defined from calibration. In the

developed program, to shorten the processing time, the distorted image was transformed on the basis of predefined lookup table images in which the destination coordinates of the x and y axis were stored.

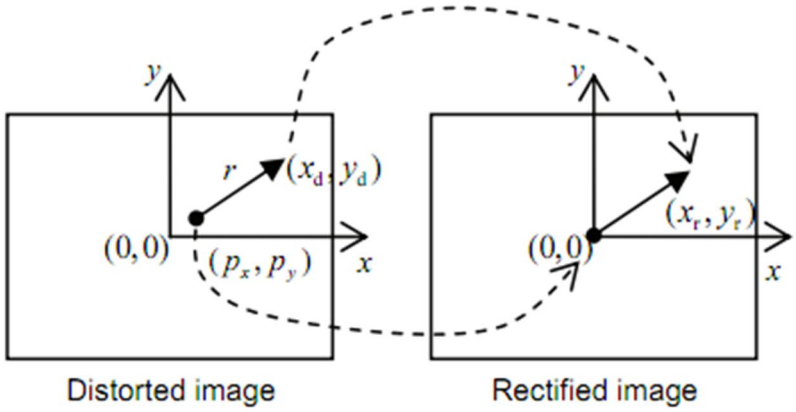


Figure 3.5 Image rectification

(2) Estimation of the camera's extrinsic parameters

The extrinsic parameters of a camera include its XYZ coordinates and the roll, pitch, and yaw angles. They can be estimated from captured images and known landmarks. A marker was placed in front of the camera and moved to different positions, and these positions were measured by a total station (TS). An accurate position of the GPS antennae, front and rear center points of the tractor, and right and left center points of the rear axle were also measured using the TS. The initial inclination of the IMU was recorded at the same time. The extrinsic parameters were calculated by comparing the coordinates of the center of the markers in an image and their real coordinates measured by the TS. Figure 3.6 is a composite photograph of 13 images of a single marker placed in different positions. In this image, the poles that supported the markers were deleted to make it easier to view. Figure 3.7 shows a 3D view of the estimation result.

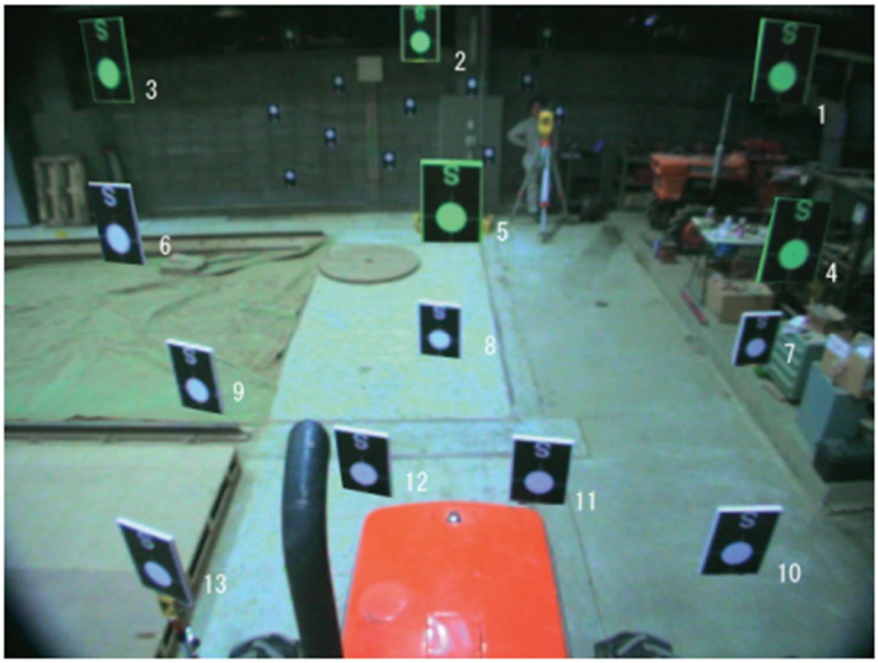


Figure 3.6 Image of the markers used to estimate the extrinsic parameters.

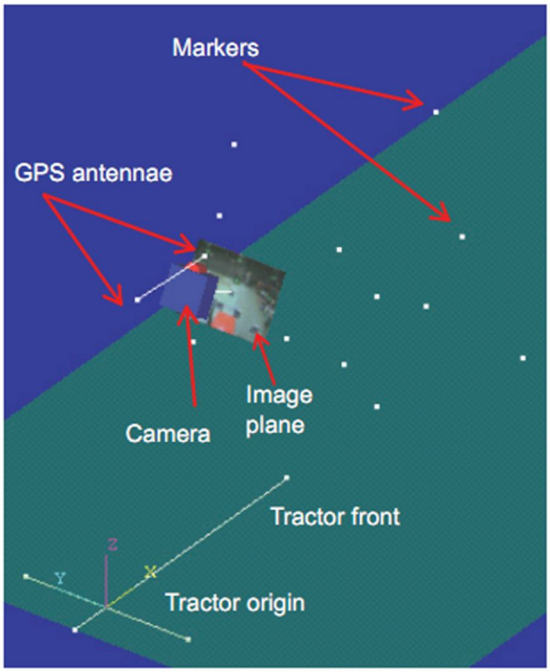


Figure 3.7 Three-dimensional view of the estimation result.

## 3.3 Results and discussion

To verify the accuracy of the match between the virtual and actual images, the following experiment was conducted. As shown in Figure 3.8, twenty-five markers were placed on corners of a 4 × 4 grid with a 2 m pitch in front of the tractor. Marker C was located at the center of the front row of the grid. The tractor was moved to different places and inclined at various attitudes. Table 3.1 shows a combination of distance, roll angle, pitch angle, and yaw angle in the experiments.

The blue and red lines drawn over the image form the virtual grid (Figure 3.8). This virtual grid was generated on the ongoing GPS and IMU data. If the position and orientation of the camera were correctly determined, the intersections of the grid would appear exactly at the center of each marker. The accuracy of camera estimation was verified by comparing the virtual grid and the markers.

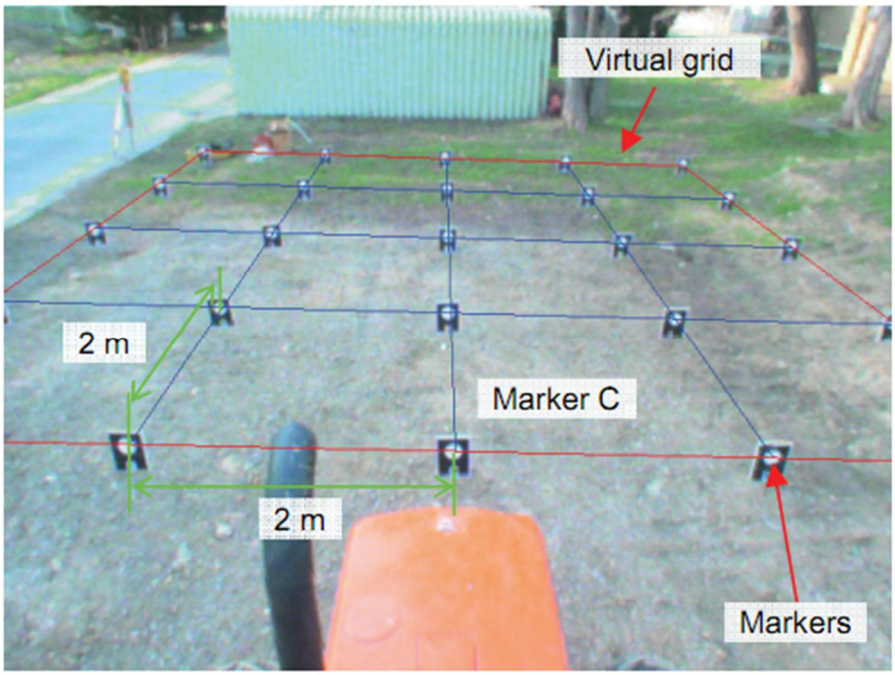


Figure 3.8 Accuracy verification of image matching.

As the positions of the markers were already known, the photogrammetric software could estimate the positions and orientations of the camera in the same way as the estimation of the extrinsic parameters. The estimated positions and orientations of the camera were compared with those estimated by the GPSes and the IMU. Table 3.2 shows the results.

Table 3.2 Accuracy of the camera position and orientation estimation.

| | X [cm] | Y [cm] | Z [cm] | Roll [°] | Pitch [°] | Yaw [°] |
|---|---|---|---|---|---|---|
| Mean | 2.49 | 0.45 | 2.89 | −0.33 | 0.35 | −0.12 |
| RMS | 2.60 | 1.26 | 3.25 | 0.34 | 0.36 | 0.34 |
| STDV | 0.78 | 1.21 | 1.54 | 0.095 | 0.088 | 0.32 |
| Max | 4.03 | 4.10 | 5.60 | 0.59 | 0.51 | 0.91 |

Considering that the horizontal and vertical accuracies of the GPSes are 2 cm and 3 cm, respectively, the errors in the X, Y, and Z axes were acceptable. The root mean square (RMS) errors in roll and pitch angles were 0.34° and 0.36°, respectively. Since the nominal accuracy of the IMU is 0.2° in roll and pitch, errors were larger than expected. However, the standard deviations of the errors were less than 0.1°. This implies that these measured angles were biased. The IMU used in this experiment was a fiber-optic gyroscope. Basically, this type of IMU consists of a drift error. If we can compensate for this error, the accuracy of the position and orientation estimation will improve. The accuracy of the yaw angle was better than expected because considering that the baseline length between the antennae was 94 cm, the 0.3° error meant that the GPS positioning error was less than 0.5 cm. By increasing the baseline length, higher accuracy can be expected.

Figure 3.9 shows the distances from the camera to the markers plotted against the

horizontal error distance in the world coordinates system between the markers and the reversely projected intersections of the virtual grid. The line indicates the average error within each one meter of horizontal distance. As the distance increased, the projection error increased simultaneously. This is because the area equivalent to 1 pixel in an image increases with an increase in distance. The error in front of the tractor was less than 5 m. In fact, assuming that an AR is used for a tractor guidance system, high accuracy is required within an area less than 10 m from the tractor. Therefore, the accuracy obtained was suitable for guidance.

Figure 3.10 shows the distances from the camera to the markers plotted against the error distance between the markers and the cross sections in the images, measured in units of pixels. The error did not increase with distance. The projection errors in images were caused solely by the error in estimating the camera's position and orientation. The averaged error was acceptable.

**Table 3.1 Position and attitude of the tractor.**

| Changing parameters | Number | Horizontal distance between the camera and marker C [m] | Roll [°] | Pitch [°] | Yaw [°] |
|---|---|---|---|---|---|
| Distance | 1 | 3.4 | −1.7 | −1.6 | −0.5 |
| | 2 | 5.8 | −0.4 | −1.7 | −0.1 |
| | 3 | 7.3 | −0.4 | −1.4 | 0.0 |
| | 4 | 7.7 | −0.8 | −1.5 | −1.1 |
| | 5 | 10.9 | −0.1 | −0.6 | −1.0 |
| Roll | 6 | 5.4 | 9.8 | −1.2 | 0.7 |
| | 7 | 5.4 | 4.2 | −1.3 | −0.5 |
| | 8 | 5.1 | −6.6 | −1.6 | −0.1 |
| | 9 | 5.6 | −11.1 | −1.4 | −0.7 |
| Pitch | 10 | 5.3 | −1.5 | 8.0 | −1.4 |
| | 11 | 5.7 | −1.0 | 3.8 | −1.2 |
| | 12 | 4.9 | −1.7 | −7.1 | −1.4 |
| | 13 | 5.3 | −1.6 | −10.6 | −1.5 |
| Yaw | 14 | 6.6 | 0.5 | −1.3 | 42.5 |
| | 15 | 6.9 | 1.2 | −1.4 | 40.3 |
| | 16 | 5.5 | 0.5 | 0.1 | 28.9 |
| | 17 | 5.9 | 0.0 | −0.5 | 26.0 |
| | 18 | 6.4 | −2.0 | −0.6 | −26.6 |
| | 19 | 6.6 | 0.0 | −0.5 | -−46.4 |

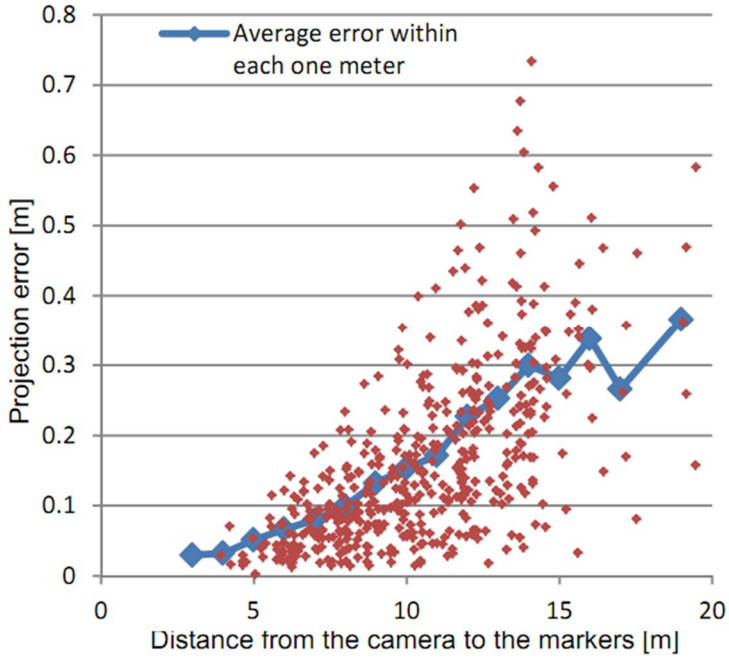


Figure 3.9 Distance from the camera to the markers plotted against the projection error distance in the world coordinates.

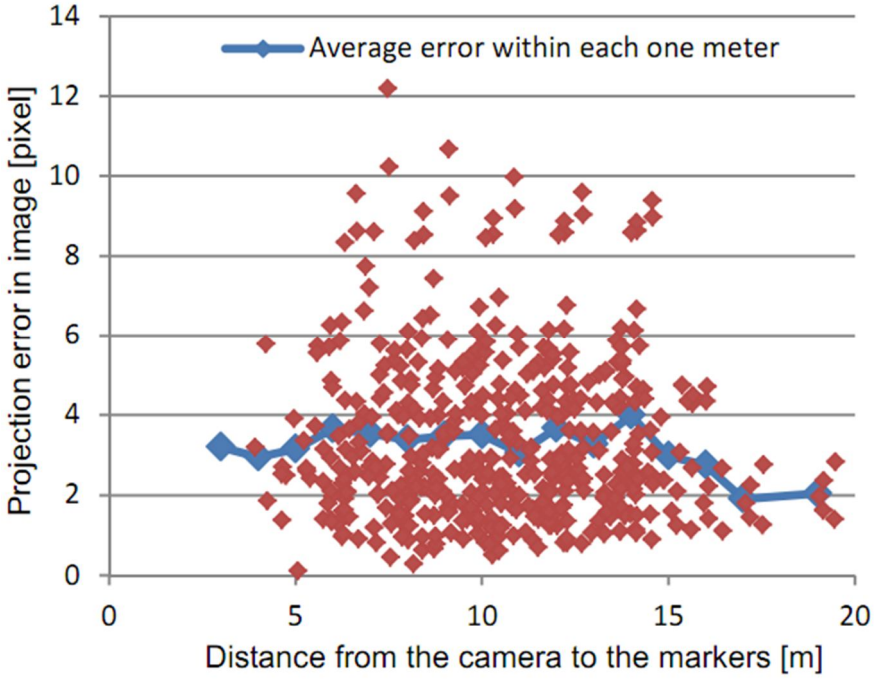


Figure 3.10 Distance from the camera to the markers plotted against the error distance between the markers and the cross sections in the image.

## 3.4 Conclusions

The following conclusions were derived from the results and discussion.

1. The developed AR system was capable of mixing a computer-generated 3D model with an actual video image in real time. The refresh frequency of the AR image was 30 Hz and the delay from image capturing to displaying was within 10 ms.

2. The position and orientation of the camera were accurately estimated using data from the two RTK-GPSes and the IMU. The estimated roll and pitch angles appeared to include bias errors.

3. The average error in distance between the markers and the intersections of the virtual grid was 3 cm, where the distance from the camera to the markers was about 3 m and 40 cm at approximately 19 m. This value was accurate enough for guidance.

4. The average error in distance between the markers and the intersections of the virtual grid in the image was 3 pixels, where the distance from the camera to the markers was about 3 m and 2 pixels at approximately 19 m. The error did not increase with distance.

# CHAPTER 4

# LASER SCANNER-BASED GUIDANCE SYSTEM FOR A COMBINE HARVESTER

## 4.1 Introduction

An AR technology has been applied on development of a human assistant guidance system for a wheel type tractor. However, this system has limitations used to the other type agricultural vehicle – combine harvester, which is widely used today for many kinds of plats such as wheat, rich, soybean, etc. Because the system needs edge information from camera using image processing method. Therefore, in order to develop a guidance system for a harvesting environment, in this chapter, a laser scanner was utilized for detect crop rows and guidance information was calculated based on the detected information of crop rows. In this study, we focused on one kind of plant – soybean. The laser scanner was chosen in this study for two reasons. At first, high accuracy of distance information could be gotten from the laser scanner without influence by the object's color. This is a great advantage for soybean harvesting, because the color of the soybean is yellowish-brown that is similar with the field color. At second, the laser scanner is an active sensor that can be used without depending on the environment illumination, therefore it can be used all the day from dawn to midnight.

In section 4.2, 3D apparatus consist of a pan tilt unit (PTU) and a laser scanner was mounted at the roof of a combine harvester will be introduced. The PTU was utilized in this study in order to wave the laser scanner in tilt direction for generating three-dimensional (3D) field information. In section 4.3, a cross correlation algorithm was utilized to detect crop row detection in a rowed crop field will be discussed. The test of the crop row detection system will be examined in section 4.4. At first, fundamental performance of the system was evaluated at laboratory conditions. And then, a field test was carried out by guidance the combine harvester to work along crop rows in a row-planted soybean field during harvesting season. Section 4.5 gives the conclusion of this chapter.

## 4.2 Research components

Figure 4.1 shows a diagram of the laser scanner-based automatic navigation system. A combine harvester (AG1100, Yanmar) that has been introduced in chapter 2 with engine power of 80.9 kW and divider width of 2.06 m was used as the platform. An integrated CAN-bus based communication network connects all sub-systems including the steering system. The key element of the automatic navigation system was a two dimension (2D) laser scanner (UTM-30LX). The PTU was used to tilt the laser scanner wave within a range of 21 degrees at 2 Hz in the vertical plane to obtain 3D field information between A and B in front of the combine harvester. A PC was used for data acquisition from the laser scanner and PTU. An RTK-GPS (Trimble MS750) and IMU (JCS-7401) measured the vehicle position and direction information for evaluating the laser scanner based guidance system.

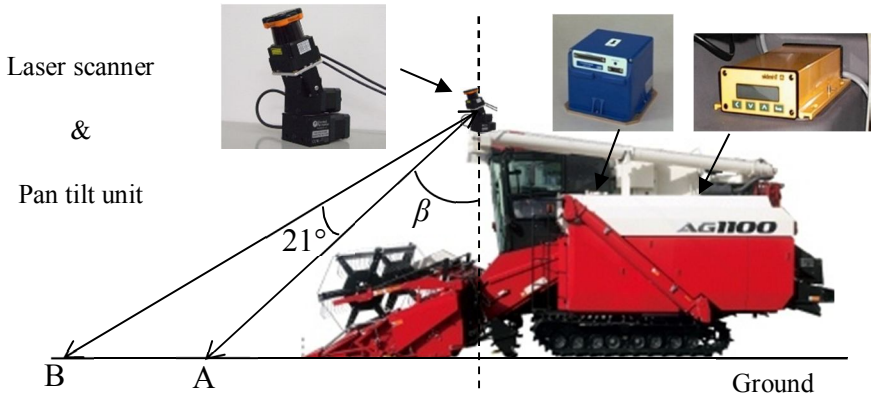


Figure 4.1 Platform and components.

The 3D data acquire process was explained by the following steps:

At first, the tilt was set to an initial tilt angle to $\beta$ degree;

At second, the tilt angle was changed to $\beta$+21 degree by a step of 3 degree, and every scanning data was acquired from the laser scanner and save to temp memory too. The data was denoted as $\Omega_i$ ($\Omega_i=\{\rho_j,\theta_j\}$, $i$=[1,2,…,8], $j$=[1,2,…,1081]); '$i$' is the scanning step index; '$\rho_j,\theta_j$' are raw data from laser scanner, '$j$' is the data index.

At third, the data $\Omega_i$ was used for the crop rows detection. The detection method will be introduced in the next section.

At fourth, the tilt angle was changed from $\beta$+21 to $\beta$ by a step of 3 degree, and the data was acquired and used for the same way. After the tilt backed to the initial angle, the next loop of detection will started. In this way, the up-down tilt rotation was continuous done in the experiment.

## 4.3 Detection method of crop rows

### 4.3.1 Soybean crop profile modeling

An understanding of the field shape is needed for navigating the combine harvester to run along crop rows. In this study, the field profile was modeled by investigating the spatial distribution of range data measured by the laser scanner in a row-planted soybean field. As shown in Figure 4.2, the laser scanner measures distances in $X_LO_LY_L$ plane under its own Laser-PTU 3D system coordinate system ($O_L$, $X_L$, $Y_L$, $Z_L$) for every scanning. The scanning values were changed from the coordinate system of laser scanner to Cartesian coordinate system by Eq. (4.1),

$$\begin{bmatrix} X_L \\ Y_L \\ Z_L \end{bmatrix} = \begin{bmatrix} \rho \cdot \cos\theta \\ \rho \cdot \sin\theta \\ 0 \end{bmatrix}, \tag{4.1}$$

where $\rho$ is the distance between the laser scanner reference origin and the object, and $\theta$ is the angle of the beam direction away from the origin axis $O_LX_L$.

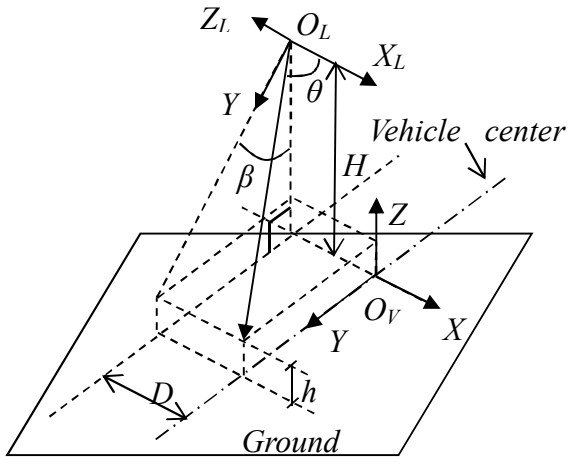


Figure 4.2 Data coordinate transformation from the laser scanner to Laser-PTU 3D system.

The coordinate system of the vehicle has its plane $X_V O_V Y_V$ on the ground plane and its origin fixed on the vehicle. By assuming that the axis $O_L X_L$ is parallel to the ground, the range data of crop plants relative to the combine harvester were obtained by rigidly transforming coordinates under the laser scanner system into the vehicle local coordinate system according to Eq. (4.2),

$$\begin{bmatrix} X_V \\ Y_V \\ Z_V \end{bmatrix} = \begin{bmatrix} \rho \cdot \cos\theta \\ \rho \cdot \sin\theta \cdot \sin\beta \\ H - \rho \cdot \sin\theta \cdot \cos\beta \end{bmatrix}, \tag{4.2}$$

where, $H$ is the height of the laser scanner origin $O_L$ above the ground ($H$ = 3 m in this study), and $\beta$ that has shown in Figure 4.1 is the angle between the scanning plane $X_L O_L Y_L$ and the vertical axis going through $O_L$. Therefore, $Z_V$ denotes the height $h$ of crop plants if the ground is assumed to be a plane.

Figure 4.3 shows an actual one-scan measurement series under the vehicle coordinate system. The measurement series is shown by black dots that depict the spatial distribution of soybean plants detected by the laser scanner. The soybean crop profile looks like an incomplete sine or square wave. It is easy to know the maximum crop height $H_C$ and the spacing $d$ between rows in a given field, which were 1 m and 0.75 m, respectively, in this study. Some outliers on the left could be discarded because of their poor accuracy. Thus, we have a series of measurements $g(i)$, $i$ = 0, ..., $N$-1 ($N$ being the number of measured points used in this study). Consequently, the field profile was modeled as a five-period square wave with a period of $P$, amplitude of $H_C$, pulse width of $W$, and no initial phase in this study. The first cycle, $f_0(x)$, can be written as Eq. (4.3),

$$f_0(x) = A[u(x) - u(x - W)], \tag{4.3}$$

where *u(x)* is a unit value at *x*.

The whole square wave function can be represented as a repetition of $f_0(x)$:

$$f(x) = f_0(x - nP),\ n = 0,\ +/-1,\ +/-2, \tag{4.4}$$

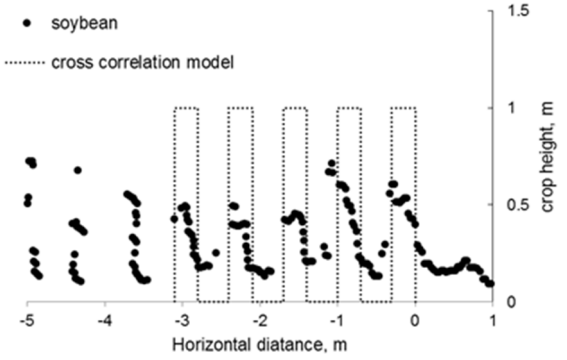


Figure 4.3 Modeling for the soybean crop profile.

4.3.2 Localization of crop rows

Since the crop profile can be represented as a square wave, it is possible to localize crop plants in the field by finding the maximum correlation $C_{max}$ between the model series $f(x)$ and field sample series $g(i)$ measured by the laser scanner. The cross correlation $C(d)$ at delay $d$ is calculated using Eq. (4.5),

$$C(d) = \frac{\sum_i (g(i) - m_g)(f(i-d) - m_f)}{\sqrt{\sum_i (g(i) - m_g)^2} \sqrt{\sum_i (f(i) - m_f)^2}}, \tag{4.5}$$

where $m_f$ and $m_g$ are the means of the corresponding series, and $f(i)$ is the $f(x)$ sample series corresponding to $g(i)$, $i = 0, 1, \ldots, N-1$. The sample points are ignored if $f(i-d)$ gets out of the range of $f(x)$.

The cross correlation is calculated for all delays $d$ = 0, 1, ..., $N$-1, resulting in a cross correlation series, of which the maximum correlation value $C_{max}$ will correspond to a delay $j$. The $x$-value of $g(j)$ is considered to be the position of the crop plant between the cut and uncut areas. In this way, all crop plants are localized under the vehicle Cartesian coordinate system.

Use of the pan tilt to rotate the laser scanner up and down in the vertical plane generates positions of crop plants that are located in the same row but at different distances away from the combine harvester. As shown in Figure 4.4, a crop plant at position $P_1$ is localized by the laser scanner at a tilt angle of 48 degrees. $P_2$ is another crop plant location detected at a tilt angle of 69 degrees. The straight line connecting $P_1$ and $P_2$ could simply be considered as the crop row separating cut and uncut areas, which is represented by Eq. (4.6) under the vehicle Cartesian coordinate system.

$$ax + by + c = 0\,, \tag{4.6}$$

where $a$, $b$ and $c$ are the straight line coefficients.

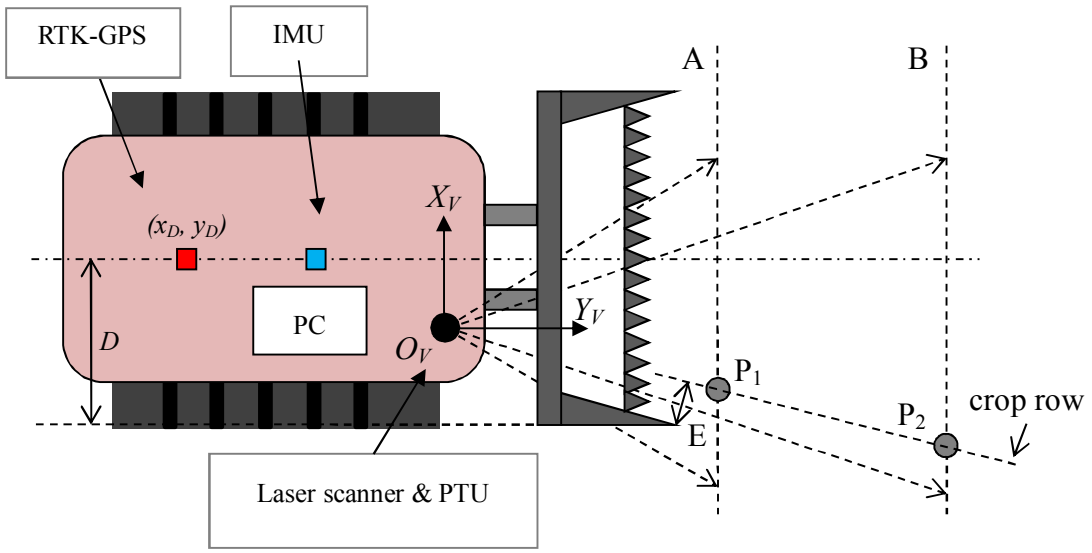


Figure 4.4 Calculation method for line of crop row.

## 4.4 Guidance parameters calculation method

During harvesting operations, the combine harvester needs to be steered following crop rows. Normally, lateral offset and heading angle error of directions of vehicle and real crop row are two important parameters to show the current vehicle position and posture error to the desired path. In this study the meaning of lateral offset ($\varepsilon$) and heading errors ($\delta_a$) are shown in Figure 4.5.

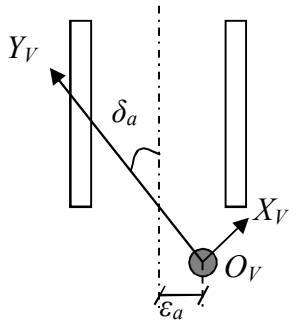


Figure 4.5 Lateral offset and heading error.

The lateral offset was calculated using Eq. (4.7).

$$\varepsilon = \frac{\left|ax_E + by_E + c\right|}{\sqrt{a^2 + b^2}}. \tag{4.7}$$

Heading error angle $\delta_a$ is the angle between the vehicle center line and the vector $\overrightarrow{P_1P_2}$, calculated using Eq. (4.8).

$$\delta = \begin{cases} \tan^{-1}\left(\frac{a}{b}\right) + \frac{\pi}{2}, if\ \frac{a}{b} < 0 \\ \tan^{-1}\left(\frac{a}{b}\right) - \frac{\pi}{2}, if\ \frac{a}{b} > 0 \end{cases} \quad \left(\frac{a}{b} \neq 0\right) \tag{4.8}$$

## 4.5 Test results and discussion

4.4.1 Test at laboratory condition

To verify the fundamental performance of the developed guidance system, the first test was conducted under laboratory conditions before field tests. The artificial target field was a flat ground with two 30-cm-high and 15-cm-wide wooden sticks placed 70 cm away from each other as shown in Figure 4.5. And the length of the artificial field was sufficient for the guidance system to move between two sticks as in an actual field.

Figure 4.6 Test of laser scanner based guidance system at laboratory condition.

In the tests, we used the guidance system to detect its lateral offset $\varepsilon$ and deflection angle $\delta$ relative to the center line between two long sticks. A total station with an accuracy of 1 cm at stationary condition was used to measure positions and directions of the sticks and the guidance system to calculate actual values of $\varepsilon$ and $\delta$ and of $\varepsilon_t$ and $\delta_t$, respectively. Table 4.1 shows the test results with the guidance system set at different positions and directions.

**Table 4.1 Test results at the laboratory condition.**

| Ground truth | | Measurements | |
|---|---|---|---|
| | | *RMSE* | |
| $\varepsilon_a$, m | $\delta_a$, deg | $\varepsilon$, m | $\delta$, deg |
| -0.3 | -15.4 | 0.02 | 0.2 |
| -0.2 | -10.3 | 0.02 | 0.2 |
| -0.1 | -5.1 | 0.01 | 0.3 |
| 0 | 0 | 0.03 | 0.2 |
| 0.1 | 5.1 | 0.02 | 0.2 |
| 0.2 | 10.3 | 0.01 | 0.2 |
| 0.3 | 15.4 | 0.01 | 0.5 |

From Table 4.1, we can see that the guidance system consisting of a laser scanner and a pan tilt unit has good accuracy in detecting artificial crop rows.

4.4.2 Test at vehicle stationary condition at a real soybean field

To evaluate the performance of the guidance system, a series of field experiments were designed and conducted in a row-planted soybean field. A combine harvester was used as the platform to carry the guidance system along crop rows for autonomous harvesting as shown in Figure 4.6.

Before the experiments, a person carried an RTK-GPS (Trimble MS750) walking along the edge crop row to record crop plant positions as reference data. The same

RTK-GPS was attached to the vehicle cab to record the vehicle trajectory after the measurement of the real position of crop rows. An IMU (JCS-7401) was used to measure the vehicle heading direction as ground truth under moving conditions simultaneously. The IMU has a drift rate of 0.5 deg/hour and an output resolution of 0.1 degrees. Since the experiment time for one autonomous run was short enough, errors originating from drifting were ignored in this study. The RTK-GPS and IMU output data at 10 Hz and the guidance system updates data at 2 Hz.

Figure 4.7 A combine harvester with the guidance system at a real soybean field.

In the first experiment, the combine harvester was stopped at the starting point to verify the repeatability of the guidance system. The relative direction and position between the vehicle and the edge crop row were measured using an RTK-GPS and IMU as reference data. Figure 4.7 shows the results under this stationary condition. The lateral error $e_\varepsilon$ fluctuated between $-0.04$ m and 0.04 m with an RMS of 0.02 m. The RMS of deflection error $e_\delta$ was 0.8 deg. Considering the inhomogeneity of shape among crop plants, even those in the same row, the guidance system showed acceptable accuracy under stationary conditions.

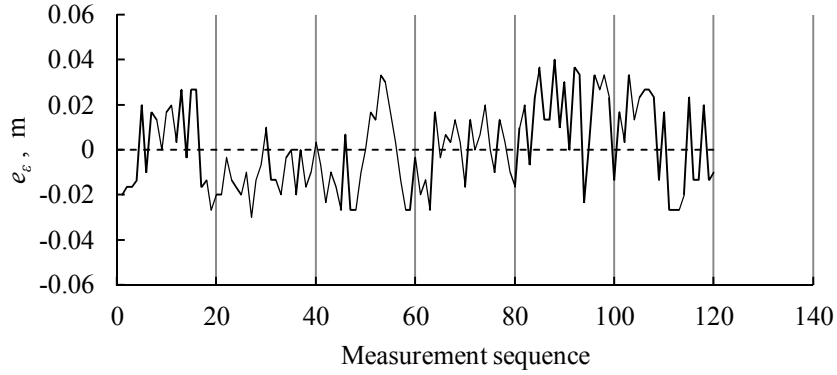


(a) Errors in lateral measurement.

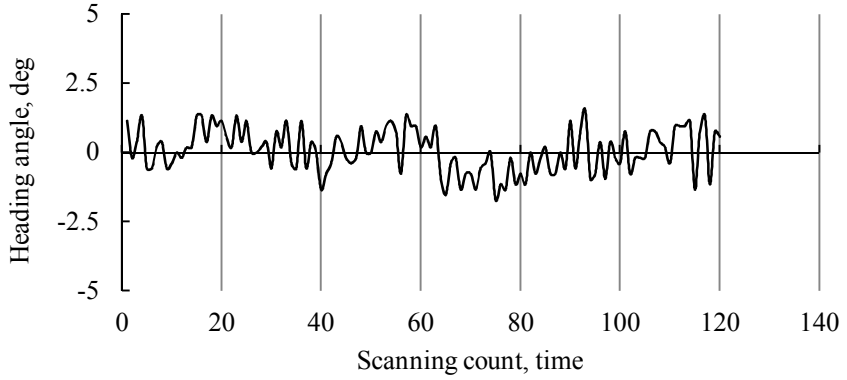


(b) Errors in heading measurement

Figure 4.8 Test results of the guidance system under stationary conditions.

### 4.4.3 Test at vehicle running conditions

In the second test, the combine harvester was driven by a farmer to verify whether the guidance system could calculate correct guidance information that refers to later offset and heading error angle. The vehicle trajectory was recorded by the RTK-GPS set at the roof of combine. Figure 4.8 shows one logged data for soybean harvesting. The soybean line is the logged position data of real soybean crop row, the combine GPS indicates the

real vehicle trajectory. The combine harvester started from point A (491424.6 m, 4744758.6 m) and ran at a speed of about 1 m/s in the test. After completing the run along the straight crop row of about 200 m, the combine harvester stopped at B (491610.9 m, 4744681.7 m).

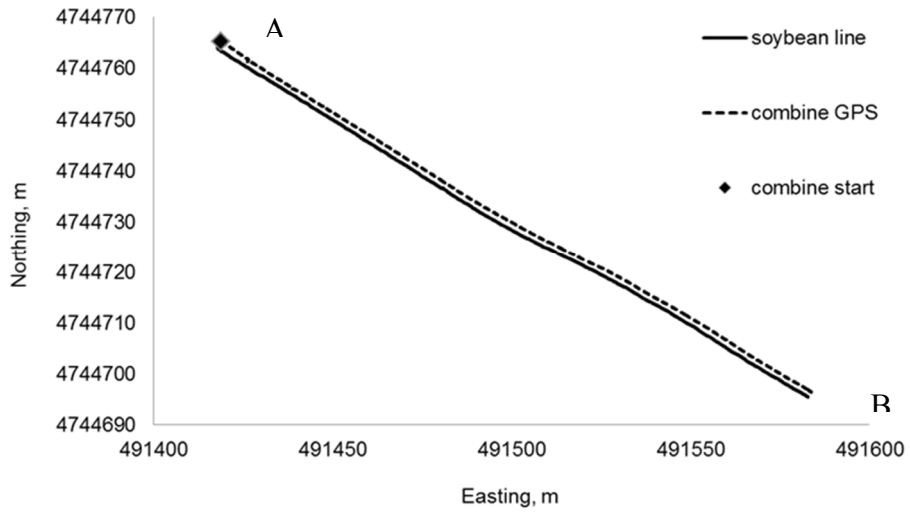


Figure 4.9 Vehicle trajectory logged by GPS and the soybean crop line.

It was noted that there was an almost constant deviation value between the vehicle trajectory and the soybean row. This is because the RTK-GPS was attached at a position of ($x_D$, $y_D$), not in line with the divider, under the vehicle coordinate system. Using the vehicle heading data obtained by the IMU, the divider position during autonomous guidance was calculated.

Figure 4.9 shows the accuracy during the running of combine harvester. In Figure 4.9 (a), we can see that the lateral offset is less than 0.2 m and its RMS is 0.07 m. For the whole autonomous run, the deflection error had an RMS of 3 degrees. Such results under moving conditions show that the performance of the newly developed guidance system is comparable to that of a manually operated vehicle during crop harvesting.

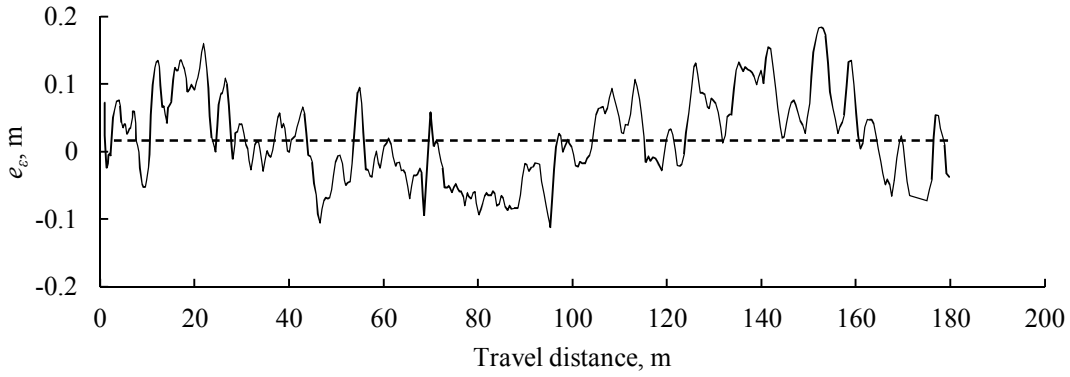


(a) Lateral error, $e_\varepsilon$

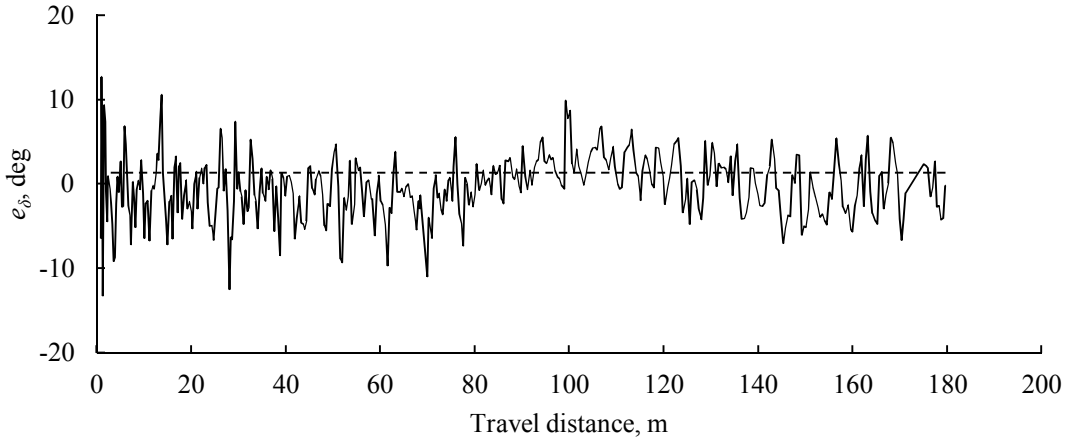


(b) Deflection error, $e_\delta$

Figure 4.10 Test results of vehicle running condition for soybean harvesting.

## 4.6 Conclusions

The feasibility of using a laser scanner-based guidance system to guide a combine harvester for autonomous runs during harvesting season was investigated in this chapter. The soybean crop profile model was created by investigating the spatial distribution of range data measured by the laser scanner. A cross correlation algorithm was used to localize the crop plants. Crop rows were estimated according to positions of crop plants

detected in the same row. Appropriate guidance parameters - lateral offset and heading angle error- were determined based on the detected crop rows. A fundamental performance test was conducted under laboratory conditions using two sticks. And the accuracy was measured by a total station. The results show that the RMS of lateral offset and heading angle error were 0.02 m and 0.8 degrees, respectively. Field tests were conducted under both stationary and running conditions of vehicle. And the results showed that the laser scanner-based guidance system could accurately localize soybean rows in the field and provide reliable guidance information at 2 Hz for the combine harvester. The RMS errors of lateral offset and heading angle were 0.07 m and 3 degrees, respectively, when the combine harvester was autonomously guided to run along the edge crop row at a speed of 1 m/s by the laser scanner based guidance system.

# CHAPTER 5

# AUTO GUIDANCE SYSTEM USING THE LASER SCANNER BASED NAVIGATION SYSTEM

## 5.1 Introduction

The previous chapter has described the hardware and algorithm on how to detect crop rows of soybean at harvesting season for soybean. And, the calculation method of lateral error and heading angle error using the information of the laser scanner of detected crop rows has been introduced. In order to extend the ability of the developed guidance system, in this chapter, a steering angle was calculated based the lateral and heading angle errors. And the steering value was sent to the combine harvester for auto guidance controlling at a soybean field.

In this chapter, a steering angle calculation method and the combine steering model were introduced in section 5.2 and section 5.3, respectively. A filed test and its results were explained in section 5.4. Finally, section 5.5 gave the conclusions of this chapter.

## 5.2 Steering angle calculation method

Because the combine harvester used in this research is a crawler type vehicle for which the moving direction of the vehicle is decided by the difference of the speed of two crawlers, the steering angle could not be send directly to the vehicle to control the

direction of the vehicle. The steering control schematic is explained in Figure 5.1.

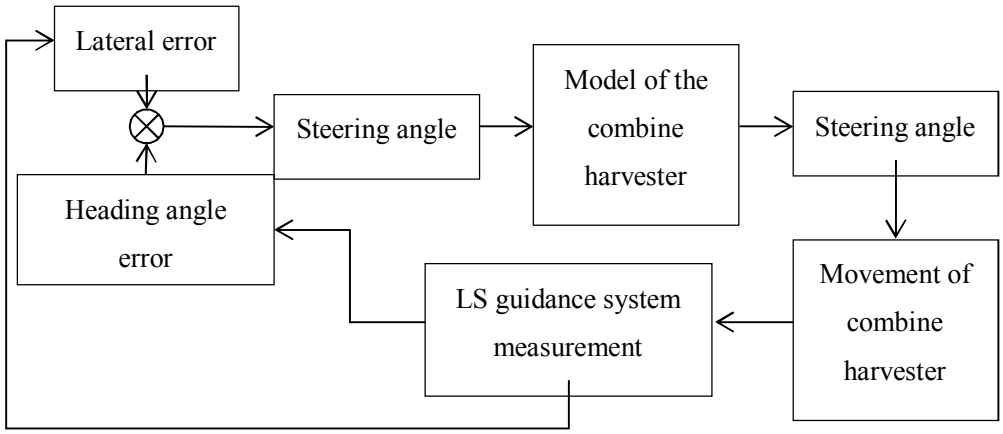


Figure 5.1 Schematic of steering control for the combine harvester.

To control the steering of the combine harvester in an automatic run, a steering controller should be designed in advance. When we have already gotten lateral and heading angle error, the steering angle of the vehicle is determined by two values – lateral error ( $\varepsilon$ )and heading error ($\Delta\varphi$) using Eq (5.1),

$$\psi = k_1\varepsilon + k_2\Delta\varphi \,. \tag{5.1}$$

where, $k_1$ and $k_2$ are corresponding gains to be tuned in field experiments, which are 3 and 5 in this study.

And then, the steering angle was transformed to a steering value by the model of the combine harvest. In this study, the model of the combine harvest refers to the relationship of the turning velocity of combine and the input steering value, and the detail is shown in the next section.

The combine harvester run to a certain direction under the steering value. Finally, the laser scanner (LS) based guidance system measured the current position and direction of the combine harvest respect to the crop rows of soybean, which calculates the lateral and heading angle errors for the next loop of control.

## 5.3 Steering control model of the combine harvester

A full-time drive system (FDS) was adopted for the driven system of the combine harvester that used in this study. The left and right crawlers could be controlled separately by two hydraulic static transmissions (HST). In this way as shown in Figure 5.2, the steering could be controlled easily at three models (AG1100, Yanmar Co. Ltd.). For the application of this study, we focused on the study of following crop rows of soybean. The first turning method – soft turning – is only considered. In this condition, the vehicle direction will be determined by the speed difference of two crawlers. The steering angle calculated at last section needs to be converted to the speed difference of two crawlers. The convention was performed by the steering ECU of the combine harvester by the maker.

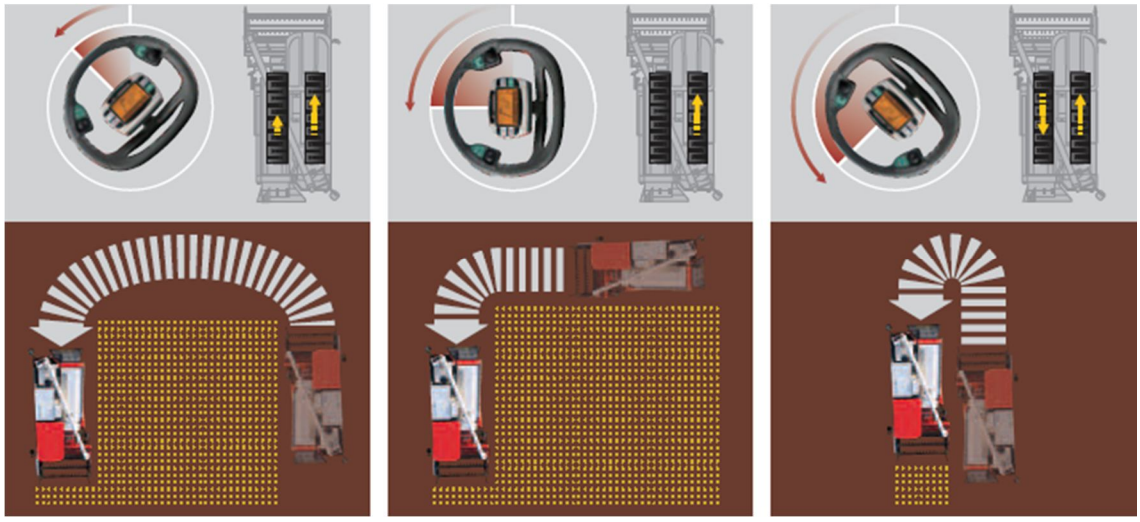

(a) Soft turning: The inner crawler speed down

(b) Brake turning: The inner crawler is stopped

(c) Spin turning: The inner crawler is rotated at reverse direction

Figure 5.2 Three kinds of steering control models for the combine harvester. (AG1100).

The relationship between steering value and turning radius of the combine harvester is shown in Figure 5.3. It can be easily seen from this figure that the relationship is

nonlinear. This relationship was measured by the company. This relationship was expressed by Eq. (5.2),

$$R = 450.5 \times |\psi|^{-1.318}, \tag{5.2}$$

where, $R$ is the turning radius; $\psi$ is the steering value ranged from -100 to +100, '-' indicates turning to left while '+' indicates turning to right.

At the 'soft turning' model, the speed of outer crawler remains the same, while the the inner speed decreases only. The speed of inner crawler could be calculated based on the turning radius by Eq. (5.3),

$$v_i = v_s \times \frac{R - l/2}{R + l/2}. \tag{5.3}$$

where, $R$ is the turning radius; $v_i$ is the speed of inner crawler; $v_s$ is the speed of the vehicle at the straight running condition; $l$, which is 1.185 m for the vehicle in this study, is the distance between of two crawlers.

And the speed of the vehicle (center of two crawlers) can be calculated by Eq. (5.4),

$$v_t = v_s \times \frac{R}{R + l/2}, \tag{5.4}$$

where, $R$, $v_s$ and $l$ are the same as Eq. (5.3); $v_t$ is the speed of vehicle.

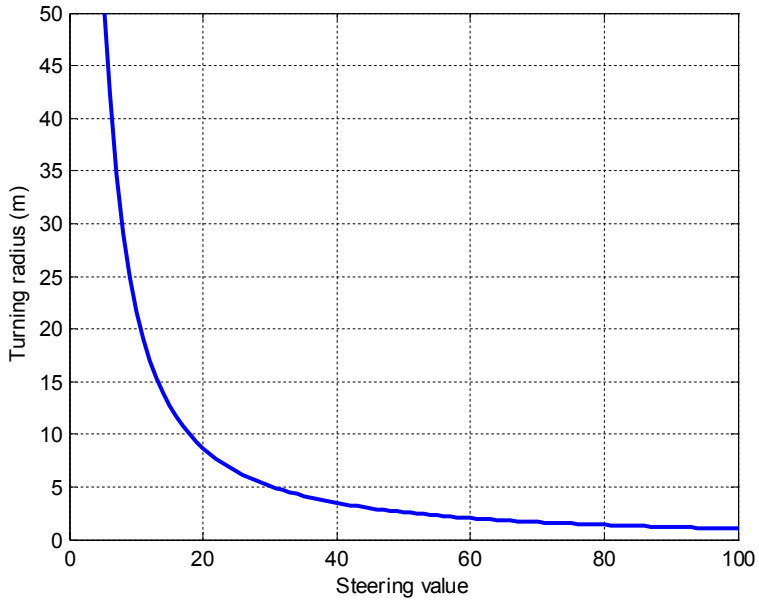


Figure 5.3 Turing radius vs steering value.

## 5.4 Field test results and discussion

In this study, the field test was conducted at a farmer's field at Kyougoku, Sapporo, Japan. Figure 5.4(a) shows the test field and Figure 5.4(b) shows the crop rows of soybean which was not so clear to be recognized. Figure 5.4 shows the experiment equipment installed at the roof of the combine harvester. The right side is the LS based guidance system. The left side is the RTK-GPS that was used to log the position of the combine in ground coordinates in order to evaluate the navigation accuracy of the LS based navigation system.

The test was carried out to follow one path without containing turning step because this system aimed to be used as auto-guidance system, instead of to be used for a fully automatic navigation system. However, we are sure that this system could be extended to perform turning navigation control if an IMU was installed to the system. This could be another research topic.

(a) (b)

Figure 5.4 Test field and crop rows of soybean.

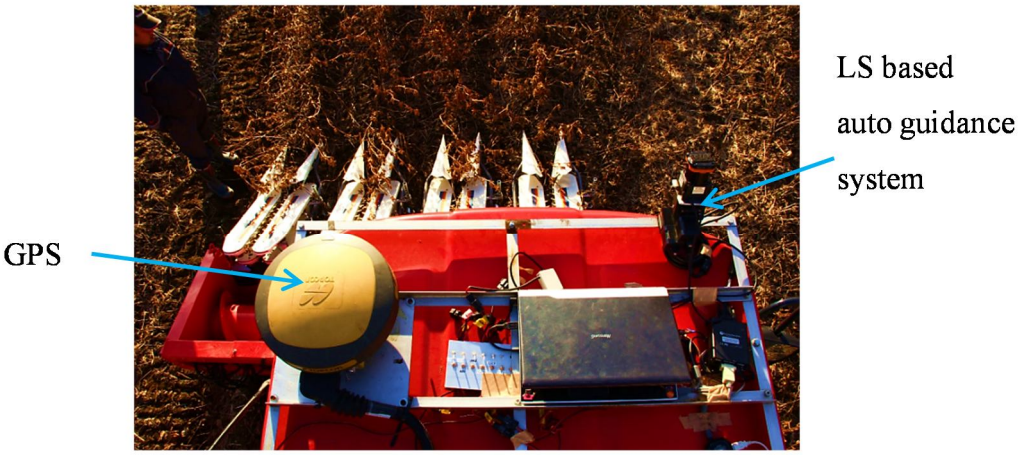


Figure 5.5 GPS and LS based auto guidance system mounted at the roof of the combine harvester.

The combine harvester was auto steered running about 135 m at a speed around 0.25 m/s at the test. In the total procedure, the lateral error, heading angle error, steering angle and GPS position were logged.

Figure 5.6 shows the vehicle trajectory and crop line of soybean that was logged by the GPS. In this figure the coordinate of the original point is [490727.22, 4743869.97] (m) in the UTM coordinate system. It can be seen that the vehicle trajectory (blue line) followed the crop line (red line) correctly, though there are some lateral errors.

Figure 5.7 and Figure 5.8 show the lateral error and heading error that calculated by the LS based auto guidance system, respectively. Both lateral and heading error were stabled around 0. Because the shape of soybean is not uniform, the lateral error is a little high. And Figure 5.9 shows the steering value that input to the combine harvester for vehicle moving direction control. This value is stabled between ±2 degrees, which mean the vehicle is continuously running forward without any sudden change of moving direction.

Figure 5.10 shows the lateral error measured by the GPS. Because the GPS receiver was a RTK-GPS whose accuracy was ± 0.02 m, the position data of the GPS could be considered as true position in the world coordinate system. Therefore, Figure 5.10 betrays the true lateral error of the LS based auto guidance system. From this figure, we can see that the maximum lateral error is near −0.5 m and the RMS value of lateral error is about 0.31 m.

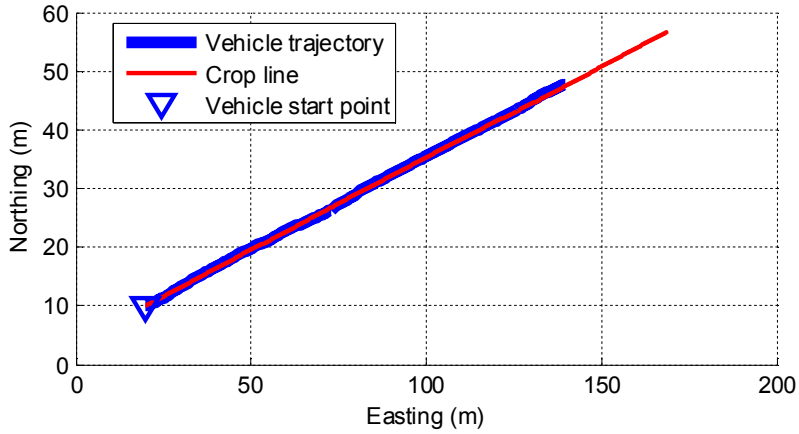


Figure 5.6 Vehicle trajectory and soybean crop line logged by the GPS.

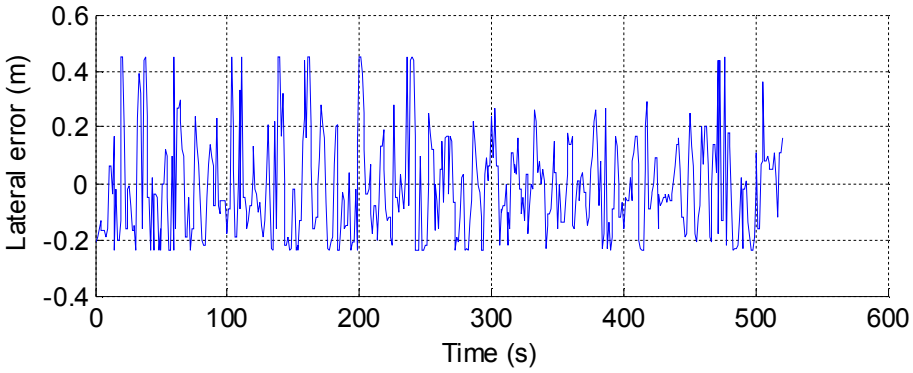


Figure 5.7 Lateral error of LS auto guidance system.

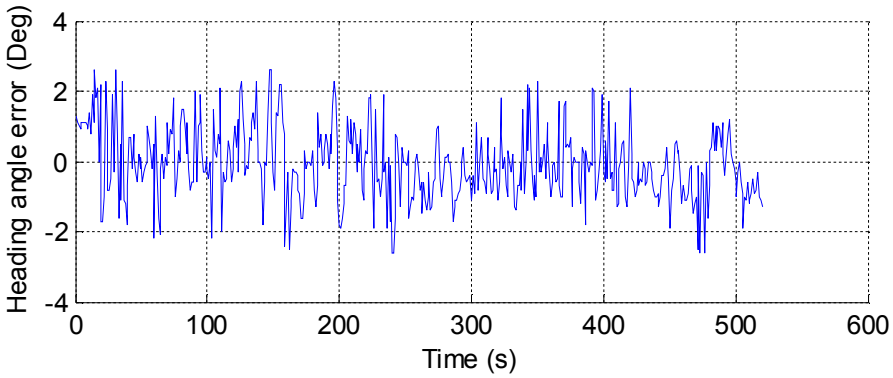


Figure 5.8 Heading angle error of LS auto guidance system.

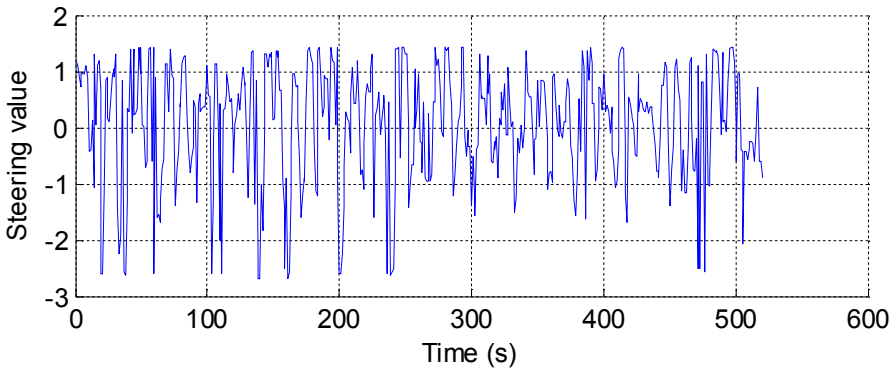


Figure 5.9 Steering value of of LS auto guidance system.

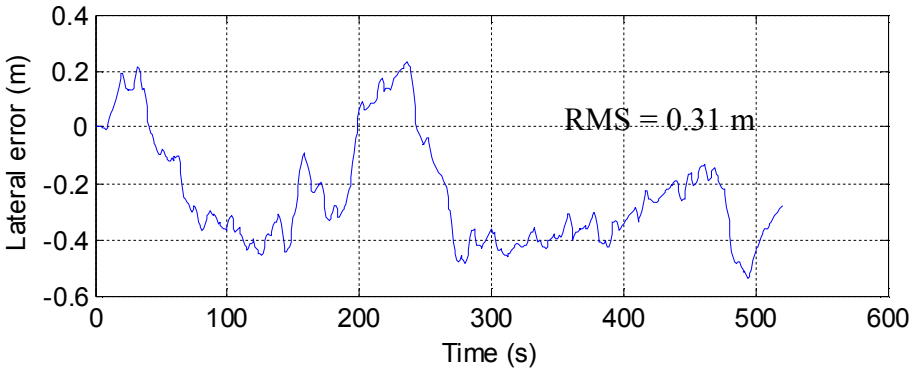


Figure 5.10 Lateral error measured by RTK-GPS.

In order to evaluate performance of the LS base auto guidance system, the other experiment using the RTK-GPS as an auto guidance sensor was conducted. Here is a brief explanation of this auto guidance system. As shown in Figure 5.11, a combine harvester is auto guided to following the navigation map. Two points from the map are always traced. One is the projection point ($P_1$) of current position ($P$); the other is a look-ahead point ($P_2$). The look-ahead distance ($L$) from $P_1$ to $P_2$ is a predetermined length. It is an adjustable value. The heading angle error ($\Delta\varphi$) is the difference between current vehicle direction and the direction from current position ($P$) to look-ahead point ($P_2$). Lateral error ($\varepsilon$) is the shortest distance from current position to the navigation map. A steering value can be calculated using Eq. (5.1).

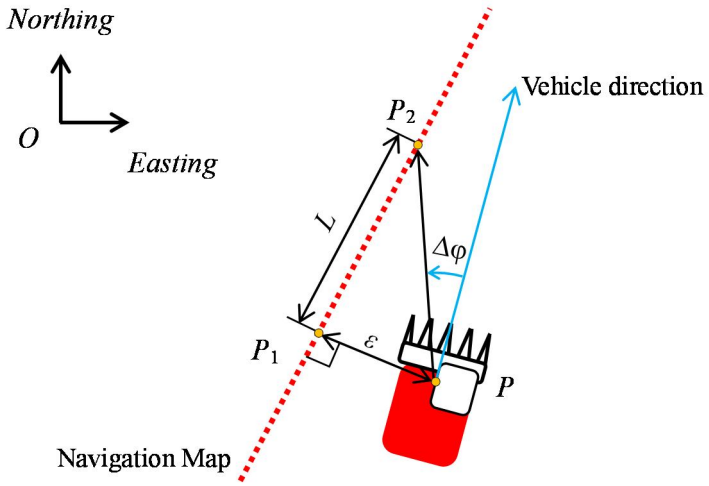


Figure 5.11 Steering value calculation method for a combine harvester using RTK-GPS.

The field test was carried out at a soybean field at Memuro, Hokkaido, Japan. The navigation path was logged by the RTK-GPS. The length of the path was around 75 m. One navigation path and a vehicle trajectory are shown in Figure 5.12. The lateral error of the RTK-GPS based auto guidance system is shown in Figure 5.12. It can be seen that the lateral error is less than ± 0.1 m. The RMS value of the lateral error is 0.04 m. It can be seen that the vehicle trajectory followed the navigation path better than in Figure 5.6 when the vehicle was navigated by the LS base auto guidance system. The reason is that the RTK-GPS has higher accuracy if the correctional signal is estimated correct.

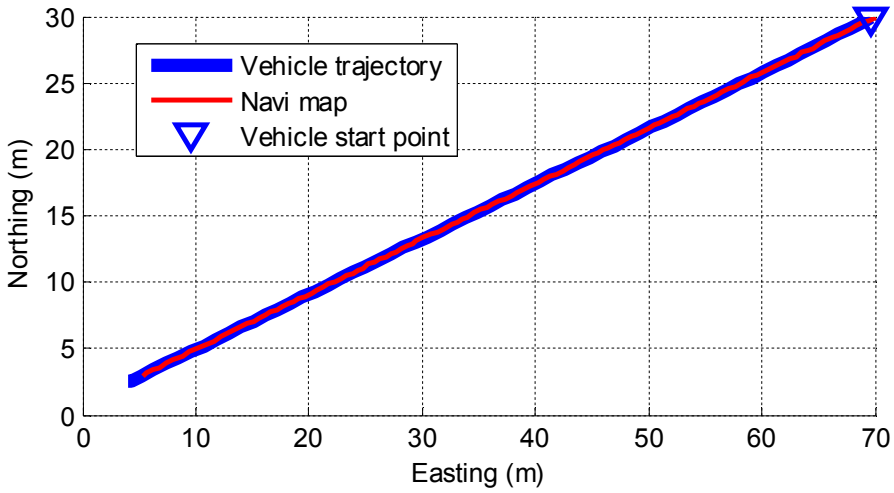


Figure 5.12 Vehicle trajectory and Navi map logged by GPS.

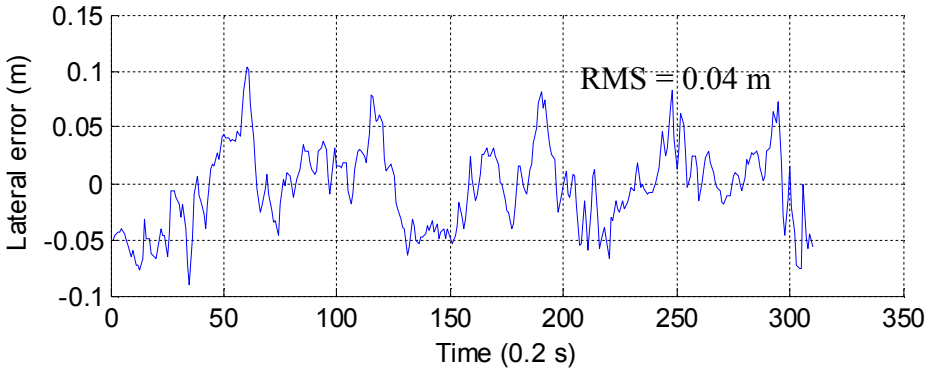


Figure 5.13 Lateral error of RTK-GPS based auto guidance system.

However, a drawback of the RTK-GPS is that RTK-GPS cannot output correct position data when the RTK-GPS system is used under trees or near buildings. Here is an example we have done at an experiment farm of Hokkaido University, Japan. Figure 5.14 shows a picture of a tractor running near trees. And Figure 5.15 (b) shows the logged position of the RTK-GPS. It can be seen that there are many position where RTK-GPS provided wrong position data. This error was caused by the GPS signal or/and the correction signals by the RTK-GPS was blocked with the trees. Figure 5.15 (a) shows the zoom-in area of the position with errors. It can be seen that the position error is as high as about 7 m. In this condition the RTK-GPS cannot be utilized for auto-guidance. In the field application of RTK-GPS based auto guidance system, the vehicle was stopped when the RTK-GPS was not 'FIX'. The FIX is a condition that RTK-GPS can provide a cm level accuracy, while 'FLOAT' and 'SINGLE' are the other two conditions of RTK-GPS that provide dm and m level accuracy position data respectively.

Figure 5.14 A vehicle is running along trees.

Therefore, at this point of view it is easier to see an advantage of the LS based auto-guidance system is that the LS is a self-contained sensor. It does not rely on outside information. Therefore, this system also meaningful for a combine harvester,

even though the accuracy is lower than the RTK-GPS based system. And consider that the width between two rows was 0.7 m; a 0.5 m lateral error could also guide the combine harvester run inside the gap of crop rows for soybean harvesting.

## 5.5 Conclusions

In this chapter, an auto guidance method based on a laser scanner and a PTU for a combine harvester was introduced. In order to control the steer angle of the combine harvester, a model for the combine harvester was described in this chapter. And an in field test was carried out at a real soybean field. The test results indicated the auto guidance method could steer the combine harvester to follow a crop row at an accuracy of 0.31 m when the vehicle speed was about 0.25 m/s. This accuracy was enough for soybean harvesting considering that the width of the crop rows was 0.7 m. The auto guidance accuracy of the laser scanner based navigation system and RTK-GPS based navigation system were also compared in this chapter. The results show that the RTK-GPS based navigation system could support better navigation accuracy. The RMS of lateral error was around 0.05 m. However, as explained in section 5.4 of this chapter, there is some place where could't get Fix solution for a RTK-GPS. In these places, the laser scanner based auto guidance system could provide an assistant solution for the RTK-GPS based navigation system, because the laser scanner was a self-contained system whose accuracy was not so much influenced by outside environment. This is an advantage of this auto guidance system.

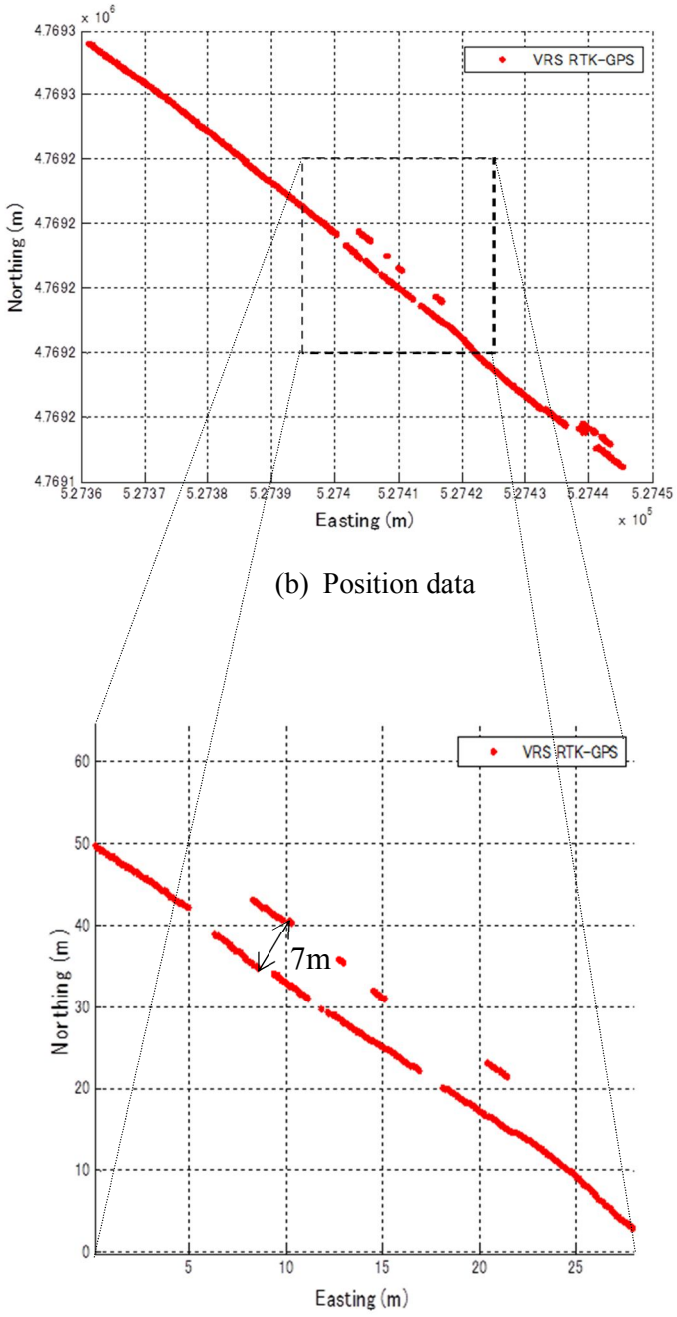


(b) Position data

(a) Zoom-in area, the original point coordinate is [527395.33, 4769174.52] (m)

Figure 5.15 The logged position data when the vehicle is running under trees.

# CHAPTER 6

# RESEARCH SUMMARY

## 6.1 Research objectives

In this dissertation, we were going to develop a guidance system for a mostly used agricultural vehicle – tractor and universal combine harvester that can be used for wheat, rice and soybean harvesting. The guidance system for the tractor was used the AR technology to create virtual guidance information merged with a real environment image from a vehicle camera. The second guidance system was used for a soybean harvesting environment using a laser scanner and PTU.

The first chapter described the background of agricultural guidance system of agricultural vehicle. And the motivation of this study is also presented. The chapter proceeds with an overview of the core concepts of the guidance system, and concludes with an outline of the dissertation.

## 6.2 Platform and sensors

This chapter discussed the equipment used in the research. This chapter started with introducing overview of the guidance system. A tractor equipped with an augmented reality (AR) navigation system composed of a GPS, a PC, and a digital color camera. They were mounted on the tractor roof. The camera interface was IEEE

1394, which allowed the camera settings to be controlled programmatically from the PC. The resolution of the image was 640×480 (pixels). The refresh frequency of the AR image was 30 Hz.

A combine harvester (AG1100, Yanmar Co., Ltd., Japan) was adopted as a test platform for a combine harvester guidance system. An integrated CAN-bus-based communication network connected the steering system, header control system and sensors for detecting harvester status, making it convenient to exchange information. The key element of the combine harvester guidance system was a laser scanner with a pan tilt control unit (PTU) mounted on the roof of the combine harvester. The PTU was used to tilt the laser scanner up and down at 2 Hz in the vertical plane to obtain three-dimensional field information in front of the combine harvester.

## 6.3 Guidance system using a camera and GPS for a tractor

This chapter discussed the camera and GPS based the guidance system for a tractor. First, developed AR system was capable of mixing a computer-generated 3D model with an actual video image in real time. The refresh frequency of the AR image was 30 Hz and the latency from image capturing to displaying was within 10 ms. Secondly, the position and orientation of the camera were accurately estimated using data from the two RTK-GPSs and the IMU. Thirdly, the average error in distance between the markers and the intersections of the virtual grid was 3 cm, where the distance from the camera to the markers was about 3 m and 40 cm at approximately 19 m. Finally, the average error in distance between the markers and the intersections of the virtual grid in the image was 3 pixels, where the distance from the camera to the markers was about 3 m and 2 pixels at approximately 19 m. The result of the accuracy evaluation

experiments value was accurate enough for guidance.

## 6.4 Laser scanner-based guidance system for a combine harvester

In this chapter, laser scanner-based guidance system for combine harvester was developed. A fundamental performance test was conducted under laboratory conditions using two sticks. The results show that the RMS of lateral offset and heading angle error were 0.02 m and 0.8 degrees, respectively. Field tests were conducted under both stationary and running conditions of vehicle. And the results showed that the laser scanner-based guidance system could accurately localize soybean rows in the field and provide reliable guidance information at 2 Hz for the combine harvester. The RMS errors of lateral offset and heading angle were 0.07 m and 3 degrees, respectively, when the combine harvester was autonomously guided to run along the edge crop row at a speed of 1 m/s by the laser scanner based guidance system.

## 6.5 Auto guidance system using the laser scanner based navigation system

An auto guidance method based on a laser scanner and PTU for a combine harvester was developed in this chapter. At first, we provided the steering value calculation method. And the steering control method was also discussed. Finally we did the test at a farmer's field. The real soybean field test results indicated the auto guidance method could steer the combine harvester to follow a crop row at an accuracy of 0.31 m when the combine harvester speed was about 0.25 m/s. This

accuracy was enough for soybean harvesting. The laser scanner based navigation system and RTK-GPS based navigation system were compared in this chapter. RTK-GPS based navigation system could support better navigation accuracy. The RMS of lateral error is around 0.05 m. But there was some place where cannot get Fix solution on a RTK-GPS. In these places, the laser scanner based auto guidance system provides an assistant solution for the RTK-GPS based navigation system, because the laser scanner is a self-contained system whose accuracy was not so much influenced by outside environment. This is an advantage of this auto guidance system.

# REFERENCES


Ahamed, T., Takigawa, T., Koike, M., Honma, T., Yoda, A., Hasegawa, H., Junyusen, P., Zhang, Q., 2004. Characterization of laser range finder for in-field navigation of autonomous tractor Automation technology for off-road equipment INTERNATIONAL CONFERENCE, Automation technology for off-road equipment; 120-130.

Alkan, R. M. and O. Baykal. 2001. Survey boat attitude determination with GPS/IMU systems. Journal of Navigation 54:135-144.

Bell, T. (1999). Automatic tractor guidance using carrier-phase differential G.P.S. Computers and electronics in agriculture: Special Issue Navigating Agricultural Field Machinery.

Bell, T. 2000. Automatic tractor guidance using carrier-phase differential GPS. Computers and Electronics in Agriculture 25, 53–66.

Benson, E.R., Reid, J.F., Zhang, Q., 2003. Machine vision-based guidance system for agricultural grain harvesters using cut-edge detection. Biosystems Engineering, 86(4), 389–398.

Buhler, D. D. 1997. Effects of tillage and light environment on emergence of 13 annual weeds. Weed Technology 11:496-501.

Buick, R. (2006). GPS Guidance and Automated Steering Renew Interest In Precision Farming Techniques, Agriculture Division, Westminster, Colorado, USA, Available at: www.trimble.com

Carmer, D.C., Peterson, L.M., 1996. Laser radar in robotics. Proc. IEEE 84 (2), 299–320.

Chateau, T., Debain, C., Collange F., Trassoudaine, L. and Alizon J. 2000. Automatic guidance of agricultural vehicles using a laser sensor. Computers and Electronics in Agriculture, 28, 243–257.

EOS Systems Inc. 2007. Radial lens distortion; Photomodeler 6 help file. Furht, B. 2011. Handbook of Augmented Reality. New York, Springer.

Fehr, B.W.; Gerrish, J.B. (1995). Vision-guided row crop follower. Appl. Eng. Agric. 11 (4), 613–620.

Gerrish, J.B., Stockman, G.C., Mann, L., Hu, G., 1985. Image rocessing for path-finding in agricultural field operations. ASAE Paper #853037, ASAE, St. Joseph, MI, USA.

Gordon, G.P., Holmes, R.G., 1988. Laser positioning system for off-road vehicles. In: Proceedings of the ASAE Meeting, Illinois, USA

Hague, T., Tillett, N.D., 2001. A bandpass filter-based approach to crop row location and tracking. Mechatronics (11), 1-12.

Han, S., Zhang, Q., Ni, B., Reid, J.F., 2004. A robust procedure to obtain a guidance directrix for vision based vehicle guidance systems. Comput. Electron. Agric. 43 (3), 179–195.

Hartmann, K. M. and W. Nezadal. 1990. Photocontrol of weeds without herbicides. Naturwissenschaften 77:158-163.

Iida, M. and Yamada, Y. 2006. Rice harvesting operation using an autonomous combine with a GPS and a FOG. Proceedings of the Conference of Automation Technology for Off-road Equipment, ASAE, 125–131.

Jiménez, A. R., Jain, A. K., Ceres, R. and Pons, J. L. 1999. Automatic fruit recognition: A survey and new results using range/attenuation images. Pattern Recognition, 32(10), 1719–1736.

John Deere Co. Ltd., 2630 greenstar 3 display. http://www.deere.com/wps/dcom/en_US /products/equipment/ag_management_solutions/displays_and_receivers/greenstar_3 _display_2630/greenstar_3_display_2630.page. 2013.

Jorge A. Heraud; Arthur F. Lange (2009). Agricultural Automatic Vehicles Guidance from Horses to GPS: Where we are going. Agricultural Equipment Technology Conference. Louisville. Kentucky. USA.

Kise, M., Zhang, Q. and Noguchi, N. 2005. An obstacle identification algorithm for a laser range finder-based obstacle detector. Trans. ASAE 48 (3), 1269–1278.

Kise, M; Zhang, Q. and Rovira, Mas F. 2005. A stereovision-based crop row detection method for tractor-automated guidance. Biosystems Engineering, 90(4), 357–367.

Larsen W.E.; Nielsen G.A.; Tyler D.A. (1994). Precision navigation with GPS. Computers and Electronics in Agriculture, 11 (1994): 85-95.

Li, M., K. Imou, K. Wakabayashi and S. Yokoyama. 2009. Review of research on agricultural vehicle autonomous guidance. International Journal of Agricultural and Biological Engineering 2:1-16.

Liao, H. E., T. Inomata, I. Sakuma and T. Dohi. 2010. 3-D augmented reality for MRI-guided surgery using integral videography autostereoscopic image overlay. IEEE Transactions on Biomedical Engineering 57:1476-1486.

Marchant, J.A., 1996. Tracking of row structure in three crops using image analysis. Computers and Electronics in Agriculture 15, 161–179.

Marchant, J.A., Brivot, R., 1995. Real time tracking of plant rows using a Hough transform. Real Time Imaging 1, 363–375.

Nagasaka, Y., Umeda, N., Kanetani, Y., Taniwaki, K. and Sasaki, Y. 2004. Autonomous guidance for rice transplanting using global positioning and gyroscopes. Computers and electronics in agriculture, 43, 223–234.

Noguchi N; Reid J F; Benson E; Will J; Stombaugh T. (1998). Vehicle automation system based on multi-sensor integration. ASAE Paper 983111. St. Joseph, MI

Noguchi, N., Kise, M., Ishii, K. and Terao, H. 2002. Field automation using robot tractor. In: Proceedings of the Automation Technology for Off-road Equipment, Illinois, USA.

Olsen, H.J., 1995. Determination of row position in small-grain crops by analysis of video images. Computers and Electronics in Agriculture (12), 147-162.

Oscar C. Barawid Jr. (2007). Development of electronic utility robot vehicle. PhD Thesis. Graduate School of Agriculture, Hokkaido University, Sapporo, Japan.

Oscar C. Barawid Jr., Akira Mizushima, Kazunobu Ishii and Noboru Noguchi. 2007. Development of an autonomous navigation system using a two-dimensional laser scanner in an orchard application. Biosystems Engineering, 96 (2): 139-149.

Parkinson, B. W.; Spilker J. J. (1996). Global Positioning System: Theory and Applications. Washington, D.C.: American Institute of Aeronautics and stronautics.

Reid, J.F., Searcy, S.W., Babowicz, R.J., 1985. Determining a guidance directrix in row crop images. ASAE Paper #85-3549, ASAE, St. Joseph, MI, USA.

Reid, J.F., Zhang, Q., Noguchi, N. and Dickson, M. 2000. Agricultural automatic guidance research in North America. Computers and Electronics in Agriculture, 25, 155-167.

Reid, J.F.; Searcy, S.W. (1987). Vision-based guidance of an agricultural tractor. IEEE Control Systems 7 (12), 39–43.

Reld, J.E. and Searcy, S. W. 1991. An algorithm for computer vision sensing of a row crop guidance directrix. Transactions of the SAE, 100 (2), 93-105.

Stombaugh, T.; Benson, E.; Hummel, J.W. (1998). Automatic guidance of agricultural vehicles at high field speeds. ASAE Paper 983110. St. Joseph, MI.

Subramanian, V., Burks, T. F. and Arroyo, A. A. 2006. Development of machine vision and laser radar based autonomous vehicle guidance systems for citrus grove navigation. Computers and Electronics in Agriculture, 53(2), 130–143.

Thorpe, C., 1990. Vision and Navigation, The Carnegie Mellon NavLab. Kluwer Academic Publishing, Dortrecht.

Tillett, N.D. 1991. Automation guidance sensors for agricultural field machines: A Review. J. Agri. Eng. Res., 50, 167-187.

Topcon Co. Ltd., System 110 is the best equipment for water-filled paddy preparation (System 110). http://www.topcon.co.jp/en/positioning/atwork/yamazaki_ag.html. 2013.

Trimble Co. Ltd., Trimble Agriculture. http://www.trimble.com/agriculture/index.aspx. 2013.

Tsubota, R., Noguchi, N., Mizushima, A., 2004. Automatic guidance with a laser scanner for a robot tractor in an orchard. In: Proceedings of the Automation Technology for Off-road Equipment, Kyoto, Japan.

Wilson J.N. 2000. Guidance of agricultural vehicles-a historical perspective. Computers and Electronics in Agriculture, 25, 3-9.

Yang Liangliang. 2013. Development of a Robot Tractor Implemented an Omni-directional Safety System. PhD Thesis. Graduate School of Agriculture, Hokkaido University, Sapporo, Japan.

Yin Xiang. 2013. Development of in field transportation robot vehicle using multiple sensors. PhD Thesis. Graduate School of Agriculture, Hokkaido University, Sapporo, Japan.

Yukumoto, O., Matsuo, Y. and Noguchi, N. 2000. Robotization of agricultural vehicles (Part 2) – description of the tilling robot. Journal of Agricultural Engineering Research, 34, 107–114.